

# Hierarchical Micro-Nano Surface Topography

## Promotes Long Term Maintenance of

## Undifferentiated Mouse Embryonic Stem Cells

*Mona Jaggy,<sup>‡,#</sup> Ping Zhang,<sup>§,¶</sup> Alexandra M. Greiner,<sup>‡</sup> Tatjana J. Autenrieth,<sup>‡,#</sup> Victoria  
Nedashkivska,<sup>§</sup> Alexander N. Efremov,<sup>§,±,†</sup> Christine Blattner,<sup>§</sup> Martin Bastmeyer,<sup>‡,#,\*</sup> Pavel A.  
Levkin<sup>§,±,\*</sup>*

<sup>‡</sup> Karlsruhe Institute of Technology (KIT), Department of Cell- and Neurobiology, Zoological  
Institute, Haid-und-Neu-Str. 9, 76131 Karlsruhe, Germany, <sup>#</sup> Karlsruhe Institute of Technology  
(KIT), Institute of Functional Interfaces (IFG), PO Box 3640, 76021 Karlsruhe, Germany,  
<sup>§</sup> Karlsruhe Institute of Technology (KIT), Institute of Toxicology and Genetics (ITG), PO Box  
3640, 76021 Karlsruhe, Germany, <sup>±</sup>University of Heidelberg, Department of Applied Physical  
Chemistry, Im Neuenheimer Feld 253, 69120 Heidelberg, Germany

<sup>\*</sup>  
Address correspondence to: levkin@kit.edu or bastmeyer@kit.edu

**Abstract:**

Understanding of stem cell-surface interactions and, in particular, long-term maintenance of stem cell pluripotency on well-defined synthetic surfaces is crucial for fundamental research and biomedical applications of stem cells. Here, we show that synthetic surfaces possessing hierarchical micro-nano roughness (MN-surfaces) promote long-term self-renewal (>3 weeks) of mouse embryonic stem cells (mESCs) as monitored by the expression levels of the pluripotency markers octamer-binding transcription factor 4 (Oct4), Nanog, and alkaline phosphatase. On the contrary, culturing of mESCs on either smooth (S-) or nanorough polymer surfaces (N-surfaces) leads to their fast differentiation. Moreover, we show that regular passaging of mESCs on the hierarchical MN- polymer surface leads to an increased homogeneity and percentage of Oct4positive stem cell colonies as compared to mESCs grown on fibroblast feeder cells. Immunostaining revealed the absence of focal adhesion markers on all polymer substrates studied. However, only the MN- surfaces elicited the formation of actin-positive cell protrusions, indicating an alternative anchorage mechanism involved in the maintenance of mESC stemness.

**Keywords:**

polymer surface, surface roughness, mouse embryonic stem cells, stemness maintenance, synthetic stem cell substrate

Pluripotent stem cells are able to differentiate into cell types of all three germ layers and possess an indefinite self-renewal capacity, which makes them promising tools for regenerative medicine, fundamental biomedical research and disease models.<sup>1-3</sup> However, the maintenance of stem cell pluripotency *in vitro* is a challenging task. The isolation of stem cells from their natural

environment usually leads to uncontrolled differentiation.<sup>4</sup> Long-term cultivation and maintenance of pluripotency is, however, a prerequisite for bringing stem cell research closer to biomedical applications. Underlying mechanisms which can help to maintain stemness *in vitro* are mostly unknown. The golden standard for maintaining pluripotency is still the culture of stem cells on feeder cell (fibroblast) layers<sup>5</sup> or the use of complex protein mixtures like Matrigel.<sup>6</sup> Cell adhesion-mediating proteins like laminin or E-cadherin,<sup>7, 8</sup> as well as immobilized Leukemia Inhibitory Factor (LIF)<sup>9, 10</sup> have also been reported to promote stemness. Major drawbacks of these systems are that they are biologically complex and poorly defined, and can lead to an increased risk of pathogenic or xenogeneic contamination.<sup>11</sup> Up till now, there are only a few completely synthetic and chemically defined stem cell culture substrates that allow long-term maintenance of embryonic stem cells (ESCs).<sup>12-15</sup> For example Villa-Diaz *et al.* reported that poly[2-(methacryloyloxy)ethyl dimethyl-(3-sulfopropyl)ammonium hydroxide] (PMEDSAH), a polymer-based zwitterionic hydrogel, could sustain human ESC (hESC) stemness for over 20 passages.<sup>15</sup> The underlying mechanisms for the influence of zwitterionic surface functionality on maintaining stemness are mostly unknown. For mouse ESCs (mESCs), a high throughput screening identified *N*-[3-(dimethylamino)propyl] methacrylamide (DMAPMA) as synthetic monomer-based substrate promoting mESC self renewal and pluripotency for at least 1 week.<sup>16</sup> Chowdhury *et al.* reported that stiffness of cell culture substrates could promote ESC pluripotency.<sup>17</sup> Numerous studies demonstrated the importance of substrate topography on the behavior and cell fate of different stem cell types.<sup>18-21</sup> Thus, substrate topography could be another important physical property for controlling embryonic stem cell maintenance.<sup>22-26</sup> For instance, it was shown that noncoated, nano rough gold layers promoted mESC pluripotency to a higher level than micro rough gold layers and to a similar level as flat gold.<sup>22</sup> Chen *et al.*<sup>26</sup> demonstrated a higher expression of the stem cell marker Oct3/4 in hESCs cultured on vitronectin-coated smooth glass surfaces compared to stem cells cultured on a corresponding nano rough glass surface. Jeon *et al.*<sup>25</sup> reported that poly-D-lysine (PDL)-coated, nanopatterned poly(dimethylsiloxane) (PDMS) culture substrates promoted self-renewal of mESCs in comparison to flat PDL-PDMS substrates. Despite this research on the influence of surface topography on ESC maintenance, the requirements for maintaining stemness are poorly understood. Furthermore contradicting results about the influence of micro- versus

nanoscale surface topography on pluripotency exist. In addition, substrates are frequently coated with proteins like gelatin or vitronectin which can cause synergistic effects and adds biochemical and thus xenogeneic components to the topographically patterned surfaces. Therefore, the long-term self-renewal and maintenance of stem cell pluripotency on a well-defined synthetic substrate is still a major challenge. Here we investigate the influence of a hierarchical micro-nano scale surface topography on the stemness maintenance of mESCs. Double scale micro-nano rough (MN-) surfaces, nano rough (N-) surfaces and smooth (S-) surfaces composed of 2-hydroxyethyl methacrylate-*co*-ethylene dimethacrylate (HEMA-EDMA) were compared. We show that only a hierarchical micro-nano surface roughness leads to enhanced long-term self-renewal (>3 weeks) of mESCs. Moreover, regular cell splitting increased the homogeneity of mESC pluripotent colonies on the MN-surface as compared to mESCs grown on a fibroblast feeder layer. Immunostaining revealed the absence of focal adhesion markers on all HEMA-EDMA substrates. Only MN-surfaces elicited the formation of actin-positive cell protrusions, indicating an alternative anchorage mechanism that is involved in maintaining the pluripotent character of mESCs.

MN-, N-, and S-surfaces were produced by UV-initiated free radical copolymerization of HEMA with EDMA in the presence of a porogenic mixture (Figure S1 in Supporting Information). Such polymerization leads to the formation of a biocompatible<sup>27</sup> porous polymer layer with a defined chemical composition. This method allows to precisely control the surface topography from micro- to nanoscale<sup>28</sup> where 2:1 and 1:4 ratios of 1-decanol to cyclohexanol in the porogenic mixture lead to the MN- and N-surfaces, respectively. The nonporous S-surface was produced by polymerizing a thin film of the methacrylate monomers in the absence of porogens. The MNsurface showed large agglomerates up to 9  $\mu\text{m}$  in height with  $919 \pm 22$  nm average surface roughness ( $S_a$ ) (Figure 1). The polymer microglobules also possessed a surface topography at the nanoscale as shown by scanning electron microscopy (SEM) (Figure 1a, bottom row; Figure S2 in Supporting Information). Due to this hierarchical topography at both nano- and microscale we term this surface micro-nano rough (MN). The N-surface consisted of a porous, sponge-like nanostructure with a roughness of  $S_a = 68 \pm 30$  nm, while the smooth surface was non-porous and flat with  $S_a = 2 \pm 0.4$  nm (Figure 1b, Figure S2 in Supporting Information). Additionally, atomic force microscopy (AFM) was performed to support the data obtained from SEM imaging and optical profilometry

(Figure S3, Figure S4 in Supporting Information). Because all three polymer surfaces are composed of cross-linked HEMA-EDMA polymers, they are not soluble in most of organic solvents or common buffers. We did not observe any visible degradation of the polymers stored in cell culture media for at least 10 days.

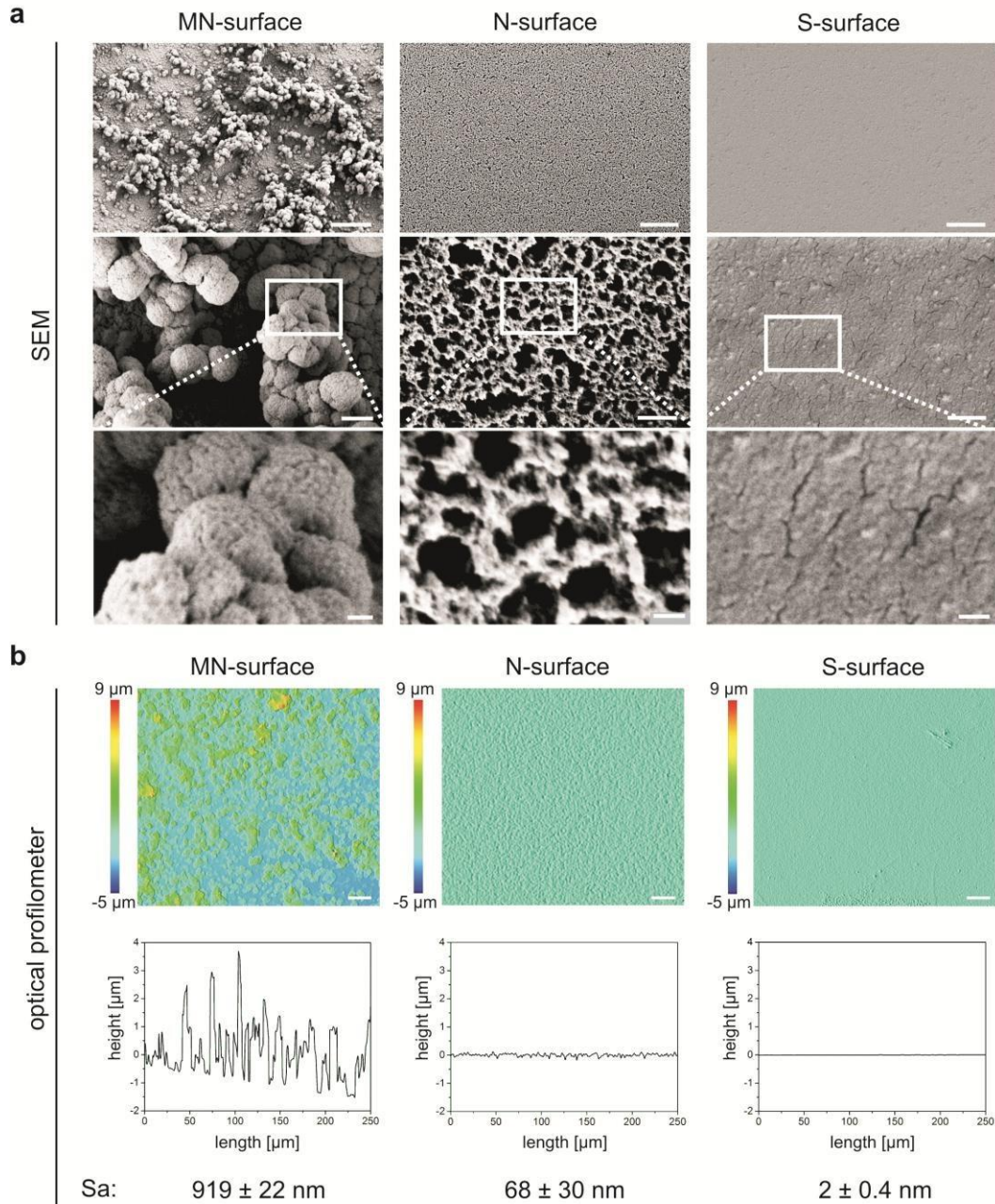


**Figure 1.** Surface characterization of HEMA-EDMA surfaces. **a**, Overview (top row) and high magnification (middle row) SEM images of MN-, N-, and S- HEMA-EDMA surfaces of different roughness. Bottom row: magnified regions as indicated (white frames in middle row). Scale bars: top row, 5  $\mu$ m; middle row, 500 nm; bottom row, 100 nm. **b**, Surface topography and roughness visualized by an optical profilometer. The look-up-tables indicate the height profile of the individual surface types. Graphs show representative line scans of the different surfaces.  $S_a$  = average surface roughness. Scale bars: 20  $\mu$ m for the MN- and N-surface; 100  $\mu$ m for the S-surface.

One of the main indications of ESC stemness *in vitro* is the number of mESC colonies expressing the pluripotency marker Oct4<sup>29</sup> whereas the outgrowth of single cells from ESC colonies is an

indication for differentiation.<sup>30</sup> We used Oct4-EGFP mESCs (mESC-Oct4EGFP),<sup>31</sup> to monitor the Oct4-expression pattern during cultivation on different surfaces. This cell line stably expresses EGFP fused to Oct4, allowing for live imaging and observation of pluripotency with the help of the fluorescent EGFP-protein. The cells were cultured in LIF-containing media on the three HEMA-EDMA surfaces as well as on glass and feeder cells as negative and positive controls, respectively. Of note, the surfaces were not coated with any cell adhesive proteins.

We first assessed the distribution of Oct4-EGFP-positive (Oct4+), Oct4-EGFP-negative (Oct4-), and mixed mESC populations on the various surfaces after 3 days of culture. The proportion of Oct4+ mESC colonies to Oct4- and mixed colonies was significantly increased for the MN-surface compared to the N-, S-surface, glass, and feeder cell surfaces (Figure 2a, b). The MN-surfaces revealed the highest percentage ( $47 \pm 2.5$  %) of Oct4+ mESC colonies while less such colonies were detected on the N-surface ( $24 \pm 2.2$  %), S-surface ( $14 \pm 6.8$  %), glass ( $16 \pm 3.2$  %), and feeder cells ( $21 \pm 6.0$  %) (Figure 2b; Chi<sup>2</sup> test, \*  $p < 0.01$ ). About 4, 5.8, and 1.6 times more of Oct4+, and thus nondifferentiated mESC colonies were found on the MN-surface in comparison to that on N-, S-surfaces and on feeder cells, respectively (Figure 2c). Additionally, total mESC colony numbers were equal between MN-surfaces, glass substrates and feeder cells, while significantly less cell colonies were observed on N- and S-surfaces (Figure 2d). These observations indicate that MN-surfaces efficiently support growth of mESC colonies. On the other hand, the single cell number was highest on glass and N-surfaces ( $\sim 10$  and  $\sim 9$  cells per mm<sup>2</sup>, respectively), while the lowest single cell number ( $\sim 4$  cells per mm<sup>2</sup>) was determined for MN-surfaces (Figure S5 in Supporting Information). Together these results suggest that HEMA-EDMA alone was not sufficient for stem cell maintenance, but MN-surface topography seemed to be a main factor for stemness maintenance. Interestingly, when mESCs were cultured without LIF on the MN-surface, the growth of mESC colonies was inhibited, while the expression of Oct4 was reduced on all tested surfaces (Figure S6 in Supporting Information).

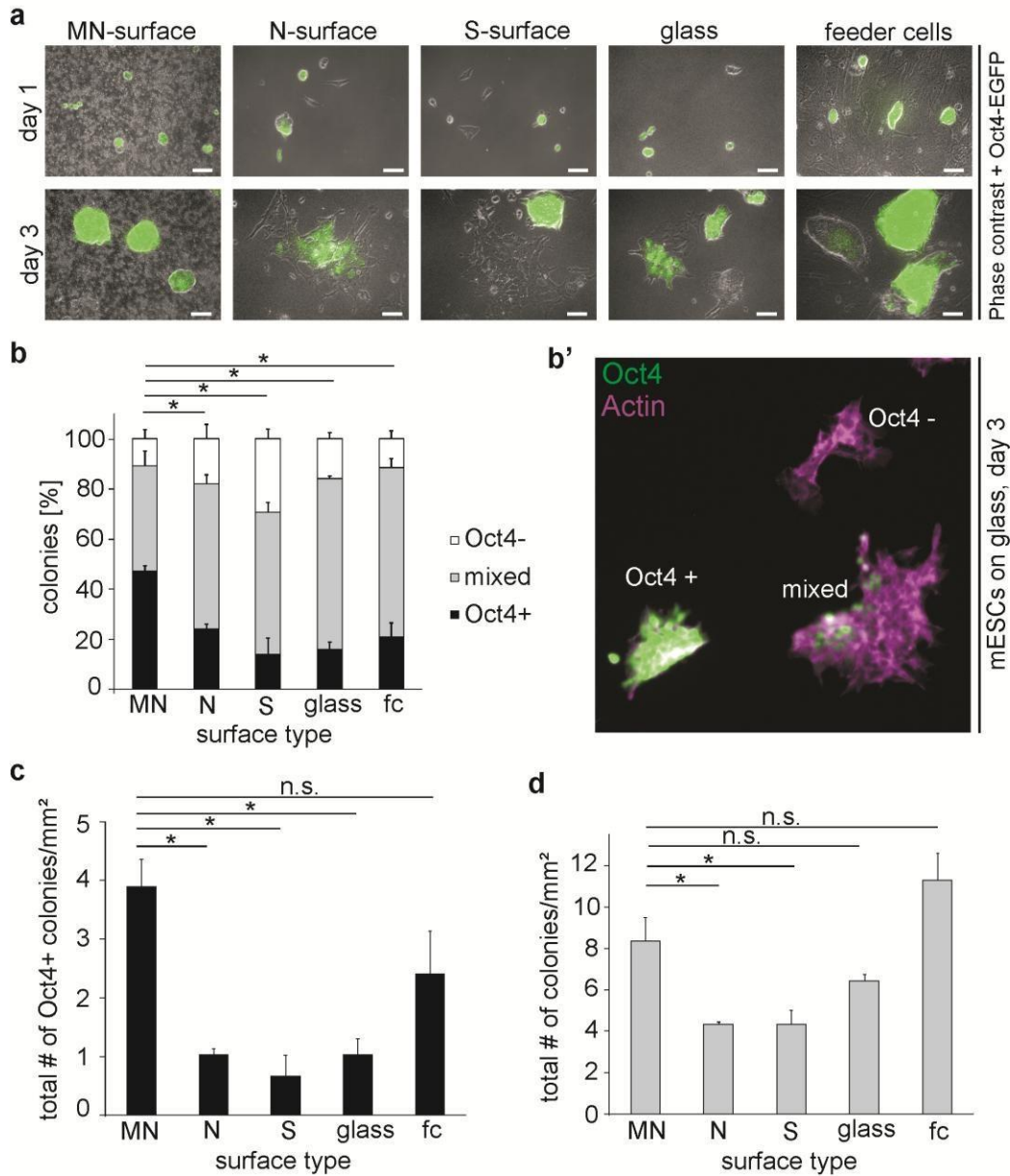


**Figure 2.** mESC-Oct4-EGFP colonies on different surfaces. **a**, Oct4-EGFP expressing mESCs were cultured in LIF-containing media for 1 or 3 days on M-, N- and S-HEMA-EDMA surfaces and on glass surfaces (negative control) or feeder cell layers (fc, positive control). Scale bars: 50  $\mu$ m **b**, Percentage of Oct4-EGFP-positive (Oct4+, black), Oct4-EGFP-negative (Oct4-, white), and mixed (gray) mESC populations on various surfaces after 3 days of culture. Chi<sup>2</sup> test; \*,  $p < 0.01$ . **b'**, Examples of Oct4+ (green), Oct4- and mixed mESC populations on a glass surface after 3 days of culture. The cells were stained for their actin cytoskeleton (magenta). **c**, Total number of Oct4+ mESC colonies on the different surfaces after 3 days of culture. Student's t-test (two-tailed); not significant (n.s.),  $p > 0.05$ ; \*,  $p \leq 0.05$ . **d**, Total number of mESC colonies on the different surfaces after 3 days of culture. Student's t-test (two-tailed); not significant (n.s.),  $p > 0.05$ ; \*,  $p \leq 0.05$ . **b, c**, and **d**,  $N = 3$ ;  $n > 200$ . All error bars represent standard error of the mean. In order to distinguish between the influence of surface topography and surface chemical properties on the Oct4-expression in mESCs, we functionalized the MN-surface either with amine groups to form a positively charged hydrophilic MN-NH<sub>2</sub> surface ( $\square_{st} 20 \pm 3^\circ$ ) or with

decanethiol to fabricate a neutral superhydrophobic MN-decyl surface ( $\theta_{\text{st}} 160 \pm 4^\circ$ ) (Table S1 in Supporting Information). The topology of all surfaces was monitored using SEM, revealing no difference between the MN-, MN-NH<sub>2</sub>-, and MN-decyl surfaces (Figure S7 in Supporting Information). Quantification of Oct4+, Oct4-, and mixed mESC colonies showed no significant difference concerning the distribution of colony types between nonmodified and NH<sub>2</sub>-modified MN-surfaces, yet a slight decrease of the percentage of Oct4+ colonies on MN-decyl surfaces was observed (Figure S7 in Supporting Information). Thus, chemical modification of HEMAEDMA seemed to be less important for stem cell maintenance than the surface topography, as long as the micro-nano rough substrate remained hydrophilic.

One of the most important properties of pluripotent stem cells is their capacity of indefinite selfrenewal<sup>32</sup> but long-term cultivation of stem cells *in vitro* often leads to spontaneous differentiation.<sup>4</sup> Therefore, one of the most important requirements for synthetic stem cell substrates is the compatibility with long-term cultivation without differentiation of ESCs. In order to compare the long-term behavior of mESCs on feeder cells with that on the MN-surface, we cultivated Oct4-EGFP expressing mESCs on both surfaces for more than 3 weeks, including LIF and regular splitting (Figure 3a). Interestingly enough, mESC colonies on the MN-surface showed a more homogeneous Oct4-EGFP distribution within colonies over time. Additionally, the circularity of the mESC colonies was determined, which represents another important indication of pluripotency<sup>32</sup> (Figure 3b). Oct4+ mESC colonies on feeder cells showed an intermediate circularity around 0.5 during the whole four-week culturing period, whereas the circularity of the colonies cultured on the MN-surface even slightly increased from 0.4 to above 0.6 over the same period (Figure 3b). We also investigated mESC growth during continuous cultivation on MN-surfaces without splitting. The MN-agglomerates were removed locally to identify the same areas over time and to observe mESC growth on detached MN-surfaces. Oct4+ mESC colonies grew continuously over time and eventually fused to form large Oct4+ colonies on MN-agglomerates (Figure 3c, white arrows). In contrast, mESCs growing in detached regions lost their Oct4-EGFP signal already after 3 days of cultivation (Figure 3c, red arrows). This important internal control showed the ease and promptness of differentiation of mESCs which did not interact with the hierarchical micro-nano rough surface topography.

To further assess the effect of MN-surfaces on mESC maintenance, we studied the expression levels of the pluripotency markers Oct4 and Nanog in mESCs cultured on MN-surfaces, Petri

dishes, and on gelatin-coated Petri dishes (Figure 3d, e) after one to four cell splitting procedures (S1-S4, passage 1-4, in Supporting Information). For these experiments, we used a second mESC line, namely D3, to proof the suitability of MN-substrates for different mESC lines and to investigate a cell system without genetic modification. Western-Blot analysis revealed that the Oct4 protein expression levels of mESCs on MN-surfaces increased over four passages (16 days). The ratio of the Oct4 levels on the MN-surface to that on the gelatin-coated or plain Petri dish was 3.2- and 2.4-fold, respectively. The levels of Nanog slightly decreased with time when mESCs were cultured on MN-surfaces, but to a much lower level as if they were cultured on gelatin or plain Petri dishes (Figure 3d, e). Long-term maintenance of stemness on MN-surfaces was further confirmed by FACS analysis. After four splitting procedures, we observed a significantly higher percentage of SSEA1-positive D3 cells cultivated on MN-surfaces as compared to cells grown on gelatin or plain Petri dishes (Figure S8 in Supporting Information). Additionally, we performed staining of alkaline phosphatase (ALP), a membrane-bound hydrolase that is highly expressed in ESCs and thus indicates the stemness of D3 mESC colonies.<sup>33</sup> We observed a strong and homogeneous ALP staining in D3 mESC colonies cultured on MN-surfaces and on feeder cells and these colonies were highly circular. In contrast, mESC colonies grown in Petri dishes with or without gelatin revealed irregularly shaped colonies as well as an inhomogeneous ALP staining (Figure S9 in Supporting Information). Overall, this indicates that the D3 mESCs started to differentiate in the Petri dish and on gelatin whereas MNsurfaces favored the mESCs growth and pluripotency.

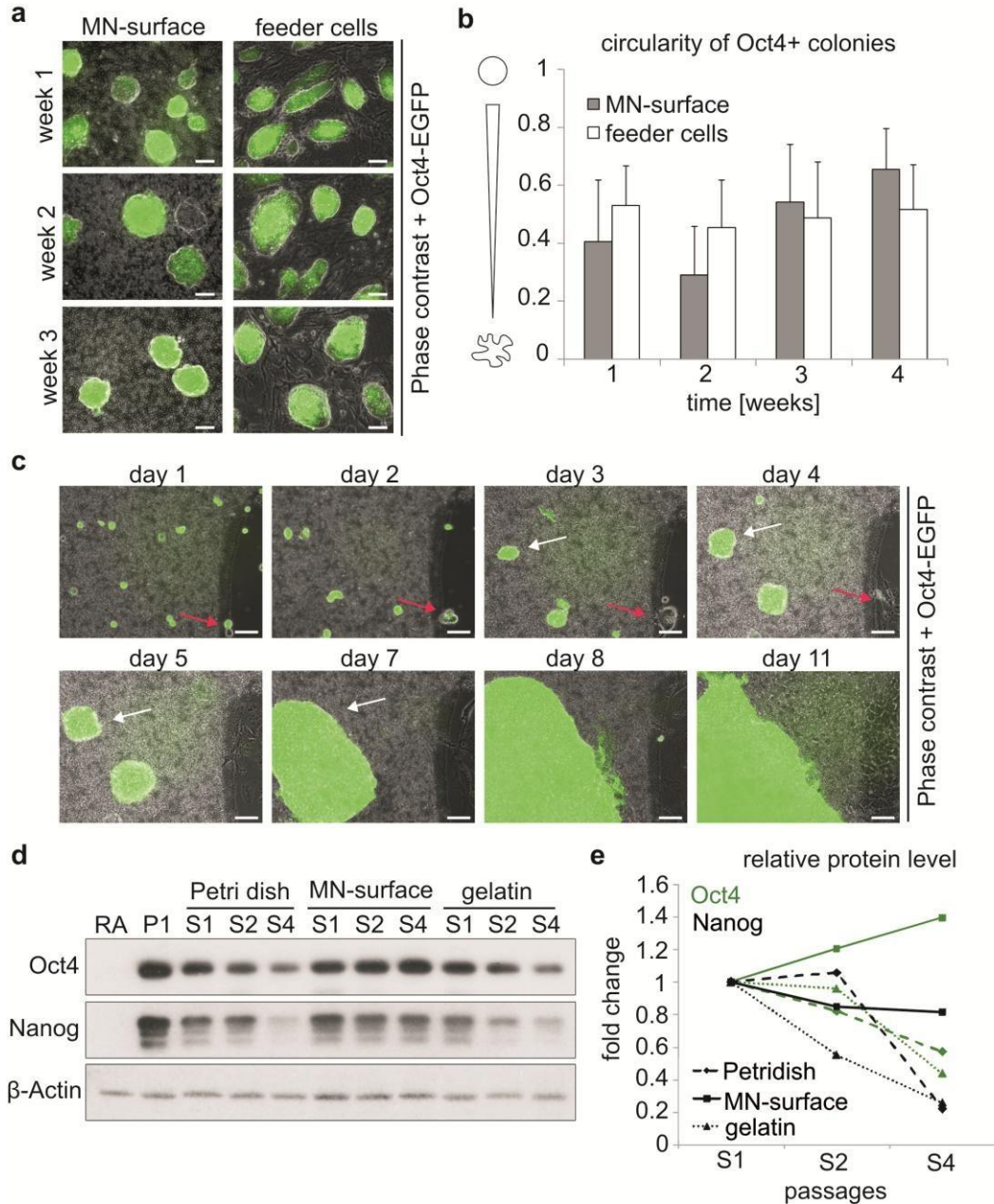


**Figure 3.** Long-term cultivation of mESCs on different surfaces. **a**, Oct4-EGFP expressing mESCs were cultivated in LIF-containing media on MN-surfaces or on feeder cell layers for 1 to 3 weeks. The mESC colonies were visualized by phase contrast microscopy and fluorescence microscopy (green, Oct4+ cells). Scale bar: 50  $\mu$ m. **b**, Circularity of Oct4+ mESC colonies on MN-surfaces and on feeder cell layers after 1, 2, 3, and 4 weeks of cultivation (including LIF and regular splitting). N = 1; n = 15-20 colonies per time point and condition. Error bars represent standard deviation. **c**, mESC-Oct4-EGFP were cultivated without splitting on a MN-surface for 11 days in LIF-supplemented growth medium. The same area was imaged over time. White arrow, example of an Oct4+ colony on MN-substrate; red arrows, example of a colony on detached part of the surface that eventually lost its Oct4signal. Scale bar: 50  $\mu$ m. **d**, Western Blot of D3 mESCs, cultured in LIF-containing media on Petri dishes, MNsurfaces, or on gelatin-coated Petri dish, respectively. The protein expression level of Oct4 and Nanog was analyzed after one to four cell splitting procedures (S1-S4). Loading control:  $\beta$ -actin; negative control: D3 mESCs differentiated in the presence of retinoic acid (RA); positive control, D3 mESCs passaged once on gelatin-coated Petri dishes (P1). **e**, Quantification of the Western Blot shown in d. Nanog- (black) and Oct4-levels (green) were normalized to the  $\beta$ -actin signal.

The results presented above demonstrate major differences between the MN- and N- and Ssurfaces with respect to mESC self-renewal. Cell-surface interactions obviously are important players in the maintenance machinery of ESC pluripotency. To obtain more insights about mESC interactions with HEMA-EDMA and control surfaces we performed SEM imaging of mESCs cultivated for 4 h on the surfaces. Single cells on MN-surfaces established thin protrusion-like extensions anchoring to the polymer agglomerates while this was rarely observed for cells cultured on the other surfaces (Figure 4a, Figure S10 in Supporting Information). Such extensions have been described before in mESCs,<sup>34</sup> but – to the best of our knowledge – have never been reported to function in ESC anchorage. Confocal microscopy revealed that the protrusions of stained mESCs on the MN-surface contained actin (Figure 4b, arrows) whereas the actin cytoskeleton was otherwise diffuse in these cells. Actin-containing protrusions could also be observed in Oct4-single mESCs (Figure S11 in Supporting Information), indicating, that they occur independently of the Oct4-level. Oct4+ mESCs on all other investigated surfaces showed no distinct actin-positive membrane extensions (Figure 4b).

It has been shown that the absence of integrin signaling favors pluripotency of ESCs.<sup>35,36</sup> To obtain more details about cell anchorage to the different substrates, single Oct4+ mESCs were stained for paxillin as a marker for integrin-mediated focal adhesions, representing the most common cell-matrix contacts.<sup>37</sup> The paxillin staining was diffuse in mESCs cultured on MN-, N- and S-surfaces and could not be detected in the membrane extensions of mESCs on MNsurfaces, indicating that HEMA-EDMA reduces focal adhesion formation. In contrast, dot-like paxillin-positive adhesion sites were identified in mESCs grown on glass and on feeder cells (Figure 4b, arrowheads). Similar results were achieved with vinculin, another cell adhesion marker (Figure S12 in Supporting Information). After 3 days in culture on MN-surfaces, mESC colonies of the Oct4- and mixed phenotype showed more prominent paxillin-clusters as compared to Oct4+ colonies (Figure S13 in Supporting Information). We additionally stained mESCs with markers for phosphorylated paxillin (pPax) and phosphorylated focal adhesion kinase (pFAK), both indicators for activated integrin signaling.<sup>38</sup> Both markers show a pronounced clustering in cells growing on glass or feeder cells (Figure S12 in Supporting Information, arrowheads), whereas cells cultivated on the three different HEMA-EDMA surfaces reveal a diffuse labeling throughout the whole cytoplasm. Regarding these results, it might be hypothesized that a reduced integrin signaling (indicated by

the absence of clustered cell adhesion markers in mESCs on HEMA-EDMA-surfaces), could help maintaining mESC stemness.

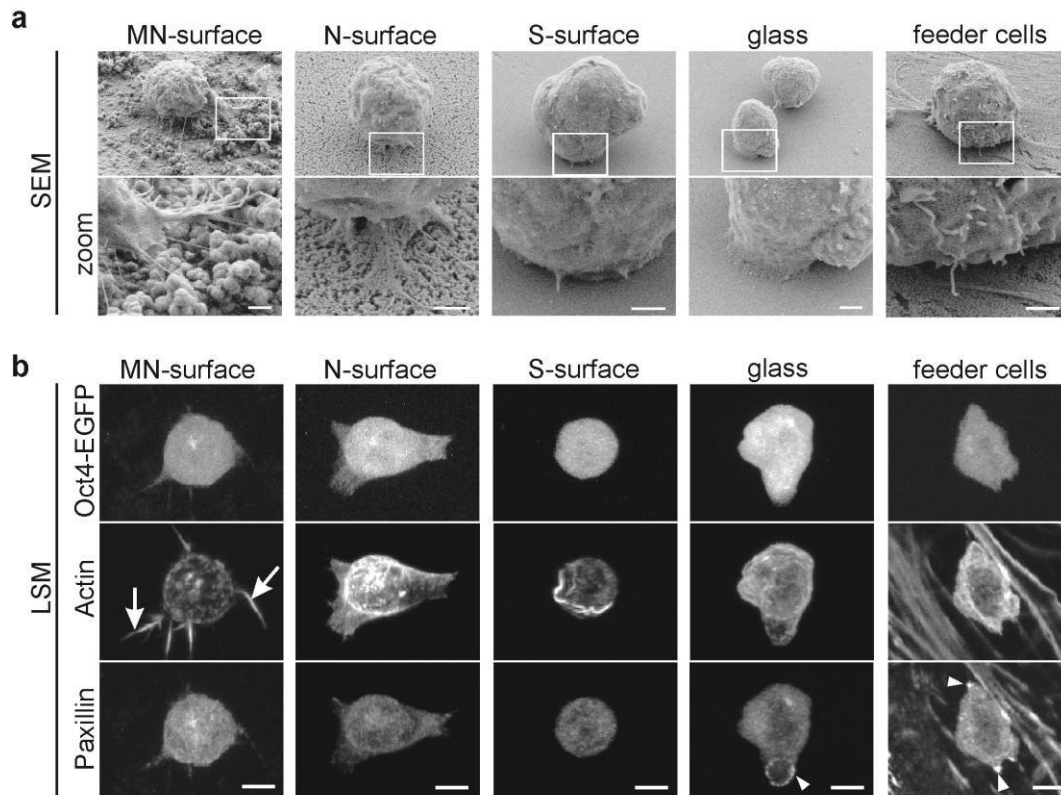


**Figure 4.** Analysis of single mESC-Oct4-EGFP morphology on HEMA-EDMA and control surfaces. **a**, Overview (top row) and zoom-in (bottom row) scanning electron microscopy (SEM) images of single Oct4-EGFP expressing mESCs adhering to HEMA-EDMA substrates of different roughness or to control surfaces (glass surface and feeder cell layers). Scale bar: 1  $\mu\text{m}$ . **b**, Fluorescence microscopy images of single Oct4-EGFP expressing mESCs on different culture substrates. The mESCs were stained for their actin cytoskeleton and paxillin (a marker of integrin positive cell-matrix adhesion sites). Arrows indicate actin protrusions; arrowheads indicate paxillin clusters. Images show maximum intensity projections of LSM-scans. Scale bar: 5  $\mu\text{m}$ .

To assess this hypothesis, we functionalized MN-surfaces with fibronectin (FN) to induce integrin signaling without changing the surface topography (Figure 5a). Interestingly, we observed the expression of endogenous FN by mESC-colonies growing on uncoated MNsurfaces (Figure 5a), which has been shown to be an additional factor favoring mESC pluripotency.<sup>39</sup> FN-functionalization significantly changed the proportion of Oct4+, Oct4-, and mixed mESC colonies with a decreased percentage of Oct4+ colonies on the FN-functionalized surface (Figure 5b). In line with this, we observed more pFAK clusters on FN-functionalized MN-surfaces compared to

nonfunctionalized MN-surfaces, indicating, that integrin-signaling was upregulated on MN-FN-surfaces (Figure 5c).

Overall, we speculate that a reduced integrin clustering in combination with actin-rich membrane extensions observed for mESCs on MN-surfaces are involved in favoring the maintenance of stemness. As the importance of stem cell anchorage, the actin-cytoskeleton and cytoskeletal tension for stem cell behavior has already been shown,<sup>40, 41</sup> an involvement of the observed actinextensions of mESCs on MN-surfaces could be quite possible.

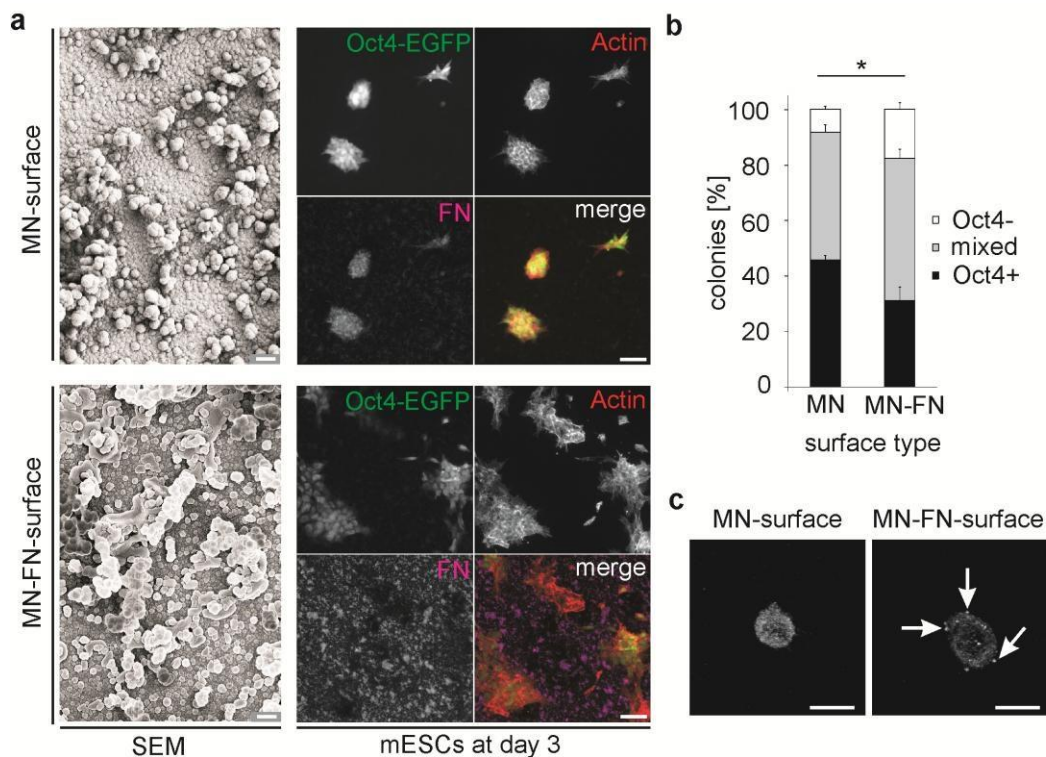


**Figure 5.** Induction of integrin-signaling on MN-surfaces. **a**, MN-surface was functionalized with fibronectin (FN) (MN-FN-surface). SEM images showing similar topographies for MN- and MN-FN-surfaces. Oct4-EGFP (white/green) expressing mESCs were cultured for 3 days on MN- and MN-FN-surfaces and the samples were stained for Actin (red) and FN (magenta). Scale bars in the SEM images: 1  $\mu$ m; Scale bars in the cell images: 50  $\mu$ m. **b**, Percentage of Oct4+ (black), Oct4- (white), and mixed (gray) mESC populations on MN- and MN-FNsurfaces after 3 days of culture. Chi<sup>2</sup> test; \*,  $p < 0.01$ .  $N = 3$ ;  $n > 200$ . Error bars represent standard error of the mean. **c**, Oct4-EGFP (white/green) expressing mESCs were cultured for 4 h on MN- and MN-FN-surfaces and stained for phosphorylated focal adhesion kinase (pFAK) as a marker for activated integrin signaling. pFAK clustering occurs predominantly on the MN-FN-surface (arrows). Scale bar: 10  $\mu$ m.

Hierarchically structured surfaces have been found to have pronounced effects in different areas, ranging from geckos showing a very efficient anchorage mechanism via hierarchically organized

hairy structures on their feet<sup>42, 43</sup> to superhydrophobicity known to be enhanced using hierarchically rough surfaces.<sup>44</sup> Here, we show another important biological effect of a surface possessing hierarchical surface topography at the micro- and nanoscale. We show for the first time that a hierarchical micro-nanoscale surface roughness favors the pluripotent character of mESCs compared to a chemically identical nano rough or smooth surface. We achieved fabrication of stem cell culture substrates that maintained stem cell self-renewal simply by their physical properties (roughness), as long as the surface chemistry remained hydrophilic. Hydrophilic MN-HEMA-EDMA surfaces efficiently supported the long-term maintenance of mESCs in LIF-containing media in contrast to N- and S-HEMA-EDMA surfaces and similar to feeder cells. We hypothesize that HEMA-EDMA surfaces restrict integrin signaling which induces mESC differentiation.<sup>35,36</sup> Only the topography of MN-surfaces allowed the formation of actin-rich protrusions, which seem to serve as an alternative and effective anchorage mechanism for mESCs into MN-HEMA-EDMA agglomerates, showing the importance of topography on mESC behavior. Feeder cells generate a complex environment including fibroblast growth factor release, noncontrolled matrix deposition, and establishment of heterologous cell-cell contacts for stem cells.<sup>45</sup> Our synthetic MN-HEMA-EDMA substrates are chemically highly defined, are easy to fabricate and can be simply utilized for stem cell studies to accomplish a less complex, feeder-free culture condition allowing more precise control over stem cell maintenance and differentiation. Thus, these substrates can be applied to gain more insights into the mechanism of stem cell pluripotency or differentiation and will be, in the long term, beneficial for biomedical applications like tissue engineering, regenerative medicine approaches, and stem cell-based therapeutics.

ASSOCIATED CONTENT

**Supporting Information Available:** Fabrication scheme, additional SEM and AFM images of HEMA-EDMA surfaces, additional quantifications of mESCs on different surfaces, images and quantification of mESCs cultivated on modified MN-HEMA-EDMA surfaces, images of ALP staining, further characterization of mESC morphology and adhesion on the different surfaces (SEM- and LSM images), water contact angle measurements, experimental procedures. This material is available free of charge *via* the Internet at <http://pubs.acs.org>.

## AUTHOR INFORMATION

### Corresponding Author

\*

Address correspondence to: [levkin@kit.edu](mailto:levkin@kit.edu) or [bastmeyer@kit.edu](mailto:bastmeyer@kit.edu)

### Present Addresses

(P.Z.) Ludwig Institute for Cancer Research, Nuffield Department of Clinical Medicine, University of Oxford, Oxford OX3 7DQ, U.K., (A.N.E.) Karlsruhe Institute of Technology (KIT), Institute of Biological Interfaces (IBG), PO Box 3640, 76021 Karlsruhe, Germany.

### Author Contributions

P.A.L., A.N.E. and V.N. had the initial hypothesis and initiated the project. M.B., P.A.L., and C.B. were responsible for the overall project management and strategy. V.N. fabricated and characterized the different surfaces. M.J., A.M.G. and T.J.A. designed the experiments with the cells and analyzed and plotted the data obtained from the cell experiments. M.J. performed the experiments with Oct4-EGFP-mESCs. P.Z. performed the studies with the D3 mESC line. A.M.G, P.L. and M.J. wrote the manuscript. All authors have given approval to the final version of the manuscript.

### Funding Sources

This work was funded by the Helmholtz Association's Initiative and Networking Fund (grant VH-NG-621) and European Research Council Starting Grant (ERC-2013-StG 337077DropCellArray).

## ACKNOWLEDGMENTS

We thank R. Kemler (MPI Freiburg, Germany) for the Oct4-EGFP mouse embryonic stem cells and D. Wedlich (KIT, Germany) for the fibroblast feeder cells, stem cell cultivation protocols and several culture requirements. B. Richter (KIT, Germany) is acknowledged for his help with sample preparation for SEM-imaging. We thank M. Hirtz (KIT, INT) for the help with AFM measurements. The research was supported by the Helmholtz Association's Initiative and Networking Fund (grant VH-NG-621) and a European Research Council Starting Grant (ERC2013-StG 337077-DropCellArray). M.J. and T.J.A. were supported by the "BioInterfaces in Technology and Medicine" Programme of the Helmholtz Association. The authors declare no competing financial interest.

## ABBREVIATIONS

AFM, atomic force microscopy; ALP, alkaline phosphatase; EDMA, ethylene dimethacrylate; ESC, embryonic stem cell; FN, fibronectin; HEMA, 2-hydroxyethyl methacrylate; hESC, human embryonic stem cell; LIF, leukemia inhibitory factor; mESC, mouse embryonic stem cell; MNsurface, micro-nano rough surface; N-surface, nano rough surface; PDMS, poly(dimethylsiloxane); pFAK, phosphorylated focal adhesion kinase; pPAX, phosphorylated paxillin; SEM, scanning electron microscopy; S-surface, smooth surface

## REFERENCES

- (1) Keller, G. *Genes Dev.* **2005**, *19* (10), 1129-1155.
- (2) Mimeault, M.; Hauke, R.; Batra, S. K. *Clin. Pharmacol. Ther.* **2007**, *82* (3), 252-64.
- (3) Sternecker, J. L.; Reinhardt, P.; Scholer, H. R. *Nat. Rev. Genet.* **2014**, *15* (9), 625-639.
- (4) Reubinoff, B. E.; Pera, M. F.; Fong, C. Y.; Trounson, A.; Bongso, A. *Nat. Biotechnol.* **2000**, *18* (4), 399-404.
- (5) Amit, M.; Itskovitz-Eldor, J. *Adv. Biochem. Eng. Biotechnol.* **2009**, *114*, 173-184.
- (6) Xu, C.; Inokuma, M. S.; Denham, J.; Golds, K.; Kundu, P.; Gold, J. D.; Carpenter, M. K. *Nat. Biotechnol.* **2001**, *19* (10), 971-974.
- (7) Miyazaki, T.; Futaki, S.; Hasegawa, K.; Kawasaki, M.; Sanzen, N.; Hayashi, M.; Kawase, E.; Sekiguchi, K.; Nakatsuji, N.; Suemori, H. *Biochem. Biophys. Res. Commun.* **2008**, *375* (1), 27-32.
- (8) Nagaoka, M.; Koshimizu, U.; Yuasa, S.; Hattori, F.; Chen, H.; Tanaka, T.; Okabe, M.; Fukuda, K.; Akaike, T. *PLoS One* **2006**, *1*, e15.
- (9) Alberti, K.; Davey, R. E.; Onishi, K.; George, S.; Salchert, K.; Seib, F. P.; Bornhäuser, M.; Pompe, T.; Nagy, A.; Werner, C.; Zandstra, P. W. *Nat. Methods* **2008**, *5* (7), 645-650.
- (10) Makino, H.; Hasuda, H.; Ito, Y. *J. Biosci. Bioeng.* **2004**, *98* (5), 374-379.
- (11) Villa-Diaz, L. G.; Ross, A. M.; Lahann, J.; Krebsbach, P. H. *Stem Cells* **2013**, *31* (1), 1-7.
- (12) Mei, Y.; Saha, K.; Bogatyrev, S. R.; Yang, J.; Hook, A. L.; Kalcioglu, Z. I.; Cho, S. W.; Mitalipova, M.; Pyzocha, N.; Rojas, F.; Van Vliet, K. J.; Davies, M. C.; Alexander, M. R.; Langer, R.; Jaenisch, R.; Anderson, D. G. *Nat. Mater.* **2010**, *9* (9), 768-778.
- (13) Irwin, E. F.; Gupta, R.; Dashti, D. C.; Healy, K. E. *Biomaterials* **2011**, *32* (29), 6912-6919.
- (14) Brafman, D. A.; Chang, C. W.; Fernandez, A.; Willert, K.; Varghese, S.; Chien, S.

- Biomaterials* **2010**, *31* (34), 9135-9144.
- (15) Villa-Diaz, L. G.; Nandivada, H.; Ding, J.; Nogueira-de-Souza, N. C.; Krebsbach, P. H.; O'Shea, K. S.; Lahann, J.; Smith, G. D. *Nat. Biotechnol.* **2010**, *28* (6), 581-583.
  - (16) Zonca, M. R.; Yune, P. S.; Heldt, C. L.; Belfort, G.; Xie, Y. *Macromol. Biosci.* **2013**, *13* (2), 177-190.
  - (17) Chowdhury, F.; Li, Y.; Poh, Y. C.; Yokohama-Tamaki, T.; Wang, N.; Tanaka, T. S. *PLoS One* **2010**, *5* (12), e15655.
  - (18) Murphy, W. L.; McDevitt, T. C.; Engler, A. J. *Nat. Mater.* **2014**, *13* (6), 547-557.
  - (19) Zhang, Y.; Gordon, A.; Qian, W.; Chen, W. *Adv. Healthc. Mater.* **2015**. DOI: 10.1002/adhm.201500351
  - (20) Dalby, M. J.; Gadegaard, N.; Oreffo, R. O. *Nat. Mater.* **2014**, *13* (6), 558-569.
  - (21) Liu, X.; Wang, S. *Chem. Soc. Rev.* **2014**, *43* (8), 2385-2401.
  - (22) Lyu, Z.; Wang, H.; Wang, Y.; Ding, K.; Liu, H.; Yuan, L.; Shi, X.; Wang, M.; Chen, H. *Nanoscale* **2014**, *6* (12), 6959-6969.
  - (23) Bae, D.; Moon, S. H.; Park, B. G.; Park, S. J.; Jung, T.; Kim, J. S.; Lee, K. B.; Chung, H. M. *Biomaterials* **2014**, *35* (3), 916-928.
  - (24) Kong, Y. P.; Tu, C. H.; Donovan, P. J.; Yee, A. F. *Acta Biomater.* **2013**, *9* (5), 6369-6380.
  - (25) Jeon, K.; Oh, H. J.; Lim, H.; Kim, J. H.; Lee, D. H.; Lee, E. R.; Park, B. H.; Cho, S. G. *Biomaterials* **2012**, *33* (21), 5206-5220.
  - (26) Chen, W.; Villa-Diaz, L. G.; Sun, Y.; Weng, S.; Kim, J. K.; Lam, R. H.; Han, L.; Fan, R.; Krebsbach, P. H.; Fu, J. *ACS Nano* **2012**, *6* (5), 4094-4103.
  - (27) Efremov, A. N.; Stanganello, E.; Welle, A.; Scholpp, S.; Levkin, P. A. *Biomaterials* **2013**, *34* (7), 1757-1763.
  - (28) Levkin, P. A.; Svec, F.; Frechet, J. M. *Adv. Funct. Mater.* **2009**, *19* (12), 1993-1998.
  - (29) Okamoto, K.; Okazawa, H.; Okuda, A.; Sakai, M.; Muramatsu, M.; Hamada, H. *Cell* **1990**, *60* (3), 461-472.
  - (30) Soncin, F.; Ward, C. M. *Genes (Basel)* **2011**, *2* (1), 229-259.
  - (31) Kirchhof, N.; Carnwath, J. W.; Lemme, E.; Anastassiadis, K.; Schöler, H.; Niemann, H. *Biol. Reprod.* **2000**, *63* (6), 1698-1705.

- (32) Thomson, J. A.; Itskovitz-Eldor, J.; Shapiro, S. S.; Waknitz, M. A.; Swiergiel, J. J.; Marshall, V. S.; Jones, J. M. *Science* **1998**, *282* (5391), 1145-1147.
- (33) Martí, M.; Mulero, L.; Pardo, C.; Morera, C.; Carrió, M.; Laricchia-Robbio, L.; Esteban, C. R.; Izpisua Belmonte, J. C. *Nat Protoc* **2013**, *8* (2), 223-253.
- (34) Baharvand, H.; Matthaiei, K. I. *Reprod. Biomed. Online* **2003**, *7* (3), 330-335.
- (35) Brafman, D. A.; Phung, C.; Kumar, N.; Willert, K. *Cell Death Differ.* **2013**, *20* (3), 369381.
- (36) Hayashi, Y.; Furue, M. K.; Okamoto, T.; Ohnuma, K.; Myoishi, Y.; Fukuhara, Y.; Abe, T.; Sato, J. D.; Hata, R.; Asashima, M. *Stem Cells* **2007**, *25* (12), 3005-3015.
- (37) Turner, C. E. *Nat. Cell Biol.* **2000**, *2* (12), E231-E236.
- (38) Robertson, J.; Jacquemet, G.; Byron, A.; Jones, M. C.; Warwood, S.; Selley, J. N.; Knight, D.; Humphries, J. D.; Humphries, M. J. *Nat. Commun.* **2015**, *6*, 6265.
- (39) Hunt, G. C.; Singh, P.; Schwarzbauer, J. E. *Exp. Cell Res.* **2012**, *318* (15), 1820-1831.
- (40) McBeath, R.; Pirone, D. M.; Nelson, C. M.; Bhadriraju, K.; Chen, C. S. *Dev. Cell* **2004**, *6* (4), 483-495
- (41) Nava, M. M.; Raimondi, M. T.; Pietrabissa, R. *J. Biomed. Biotechnol.* **2012**, *2012*, 797410.
- (42) Autumn, K.; Sitti, M.; Liang, Y. A.; Peattie, A. M.; Hansen, W. R.; Sponberg, S.; Kenny, T. W.; Fearing, R.; Israelachvili, J. N.; Full, R. J. *Proc. Natl. Acad. Sci. USA* **2002**, *99* (19), 12252-12256.
- (43) Greiner, C.; Arzt, E.; del Campo, A. *Adv. Mater.* **2009**, *21*, 479-482.
- (44) Jiang, L.; Zhao, Y.; Zhai, J. *Angew. Chem. Int. Ed. Engl.* **2004**, *43* (33), 4338-4341.
- (45) Eiselleova, L.; Peterkova, I.; Neradil, J.; Slaninova, I.; Hampl, A.; Dvorak, P. *Int. J. Dev. Biol.* **2008**, *52* (4), 353-363.

## – Supporting Information –

‡ Karlsruhe Institute of Technology (KIT), Department of Cell- and Neurobiology, Zoological

Institute, Haid-und-Neu-Str. 9, 76131 Karlsruhe, Germany, # Karlsruhe Institute of

Technology (KIT), Institute of Functional Interfaces (IFG), PO Box 3640, 76021 Karlsruhe, Germany, §Karlsruhe Institute of Technology (KIT), Institute of Toxicology and Genetics (ITG), PO Box 3640, 76021 Karlsruhe, Germany, †University of Heidelberg, Department of Applied Physical Chemistry, Im Neuenheimer Feld 253, 69120 Heidelberg, Germany

\* Address correspondence to: [levkin@kit.edu](mailto:levkin@kit.edu) or [bastmeyer@kit.edu](mailto:bastmeyer@kit.edu)

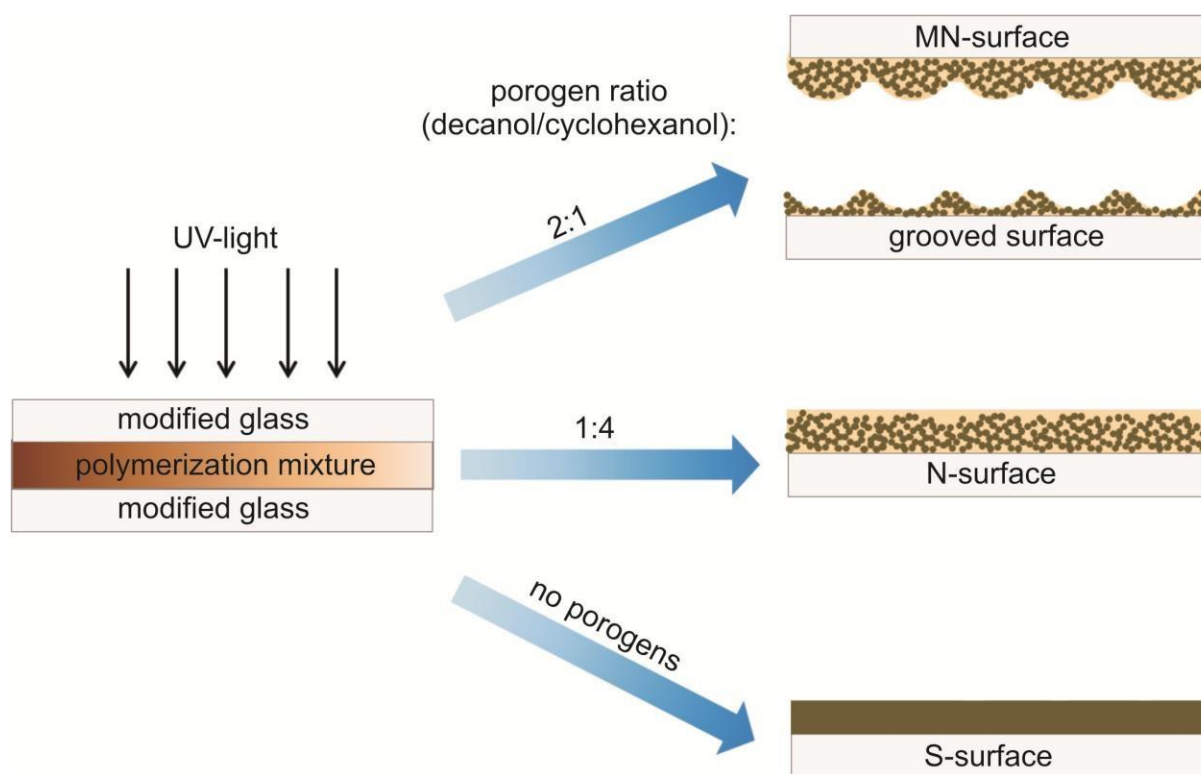


**Figure S1.** Fabrication of topographical HEMA-EDMA surfaces. Porous polymer films (MN-, N-, and S-surfaces) were fabricated by photo-polymerization of a polymerization mixture containing the monomer 2-hydroxyethyl methacrylate (HEMA), the cross-linker ethylene dimethacrylate (EDMA) and eventually the porogens cyclohexanol and 1-decanol. The porogen presence and ratio determined the outcome of surface roughness. The reaction was initiated by the photo-initiator 2,2-dimethoxy-2-phenylacetophenon (DMPA).

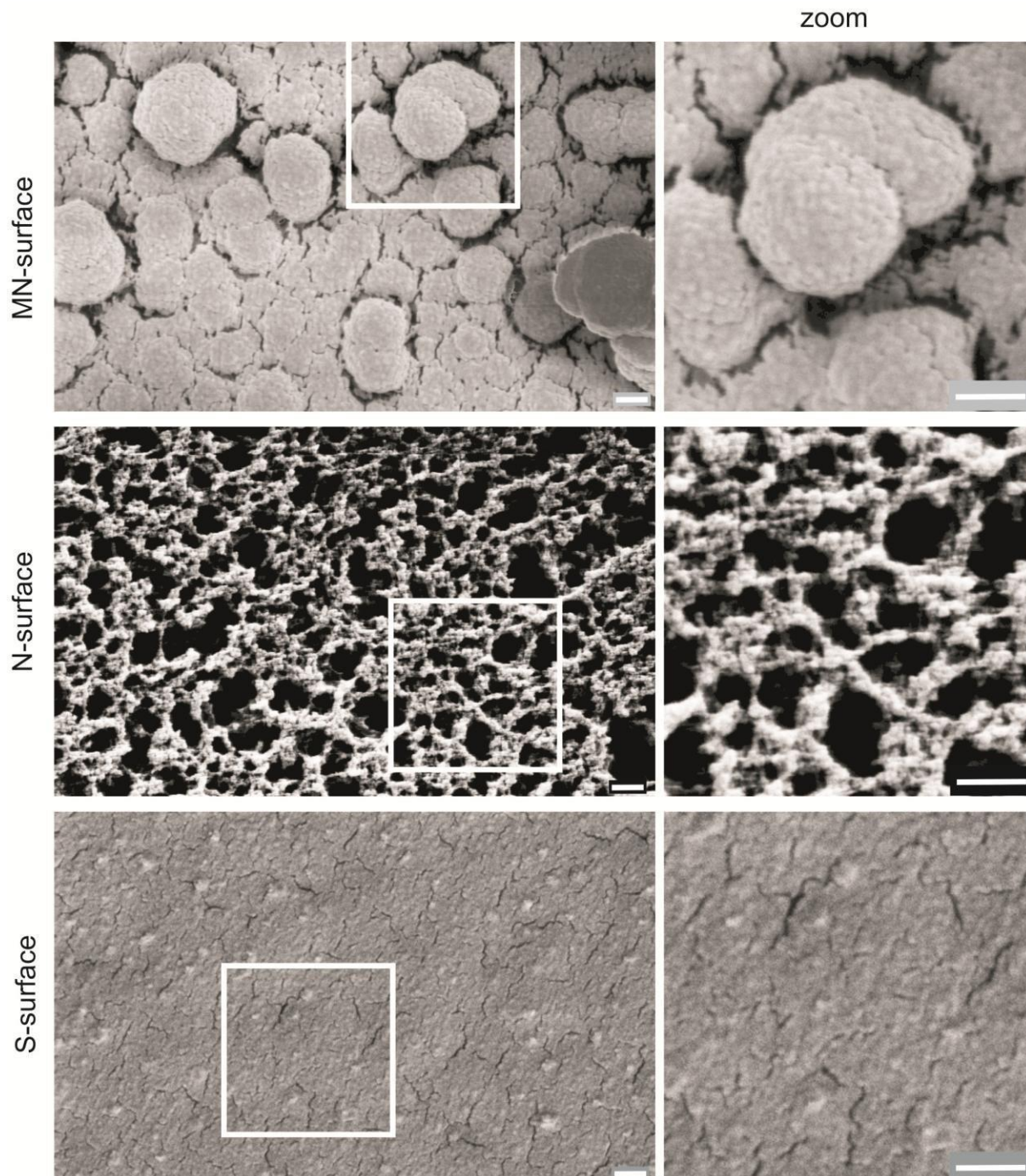


**Figure S2.** Overview (left) and high magnification (right) SEM images of MN-, N- and S-surfaces. MN-surfaces show a hierarchical roughness: the relatively large micro-globules are also textured at lower scale. N-surfaces show a porous phenotype and S-surfaces are flat. All scale bars: 200 nm.

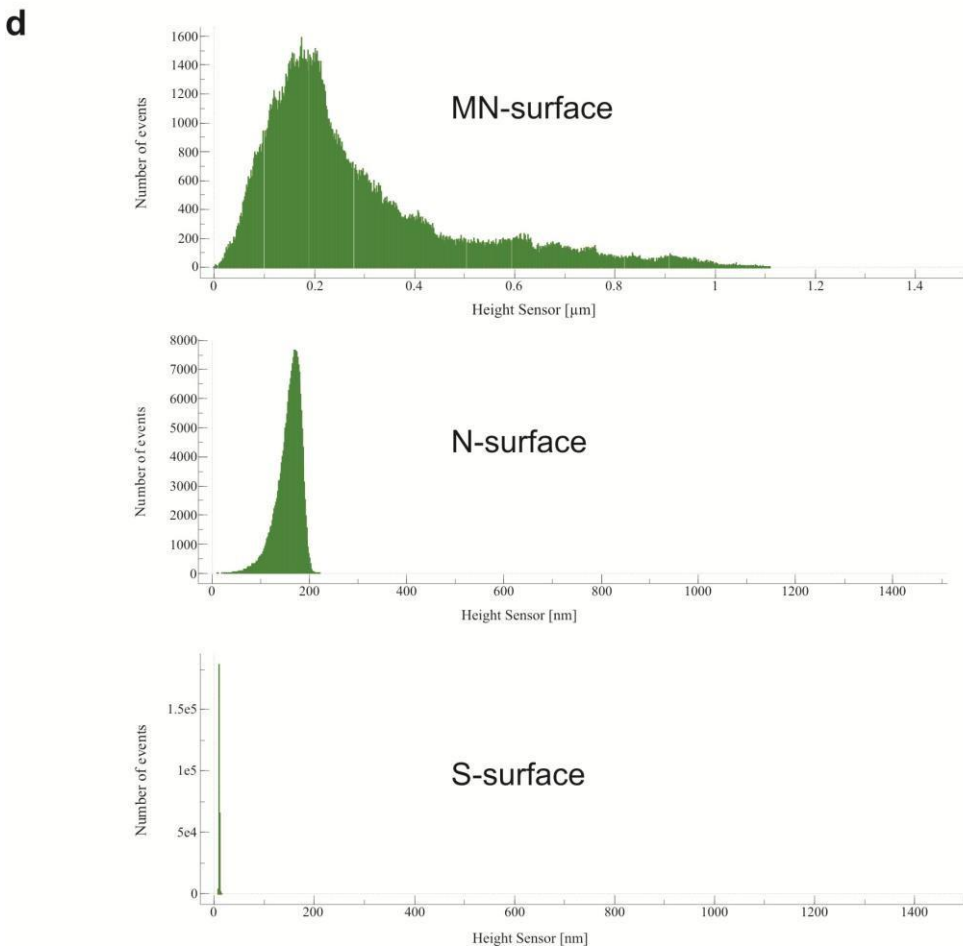
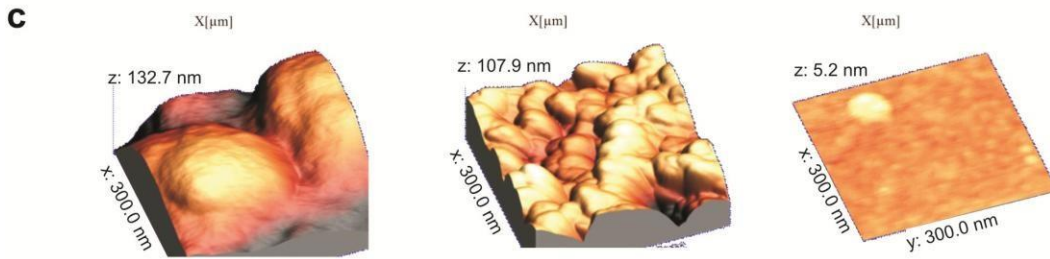
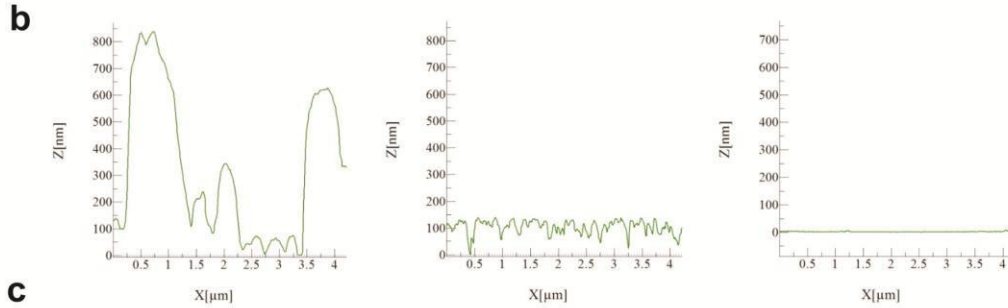
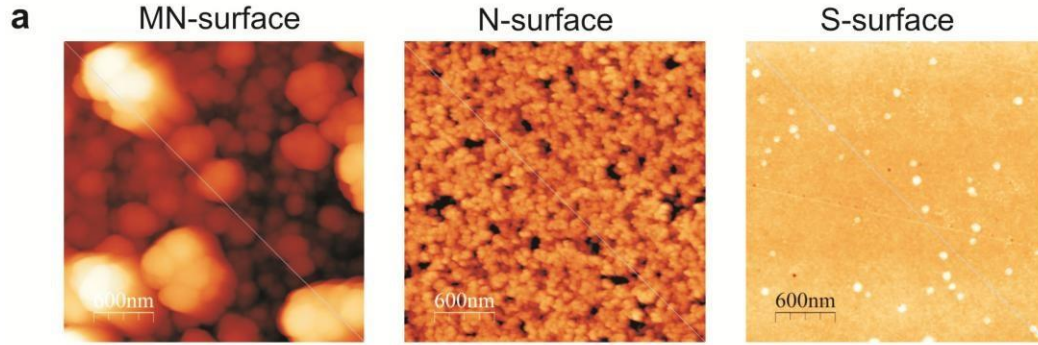


**Figure S3.** Comparison of surface topographies of MN-, N- and S-surfaces analyzed by Atomic Force Microscopy (AFM). **a**, AFM images, field of view  $3\ \mu\text{m} \times 3\ \mu\text{m}$ , tapping mode. **b**, Surface profiles (lines are indicated in **a**). **c**, AFM images 3D representation, field of view  $300\ \text{nm} \times 300\ \text{nm}$ , tapping mode. **d**, Number of events of different heights for MN-, N- and S-surfaces, measured by AFM.

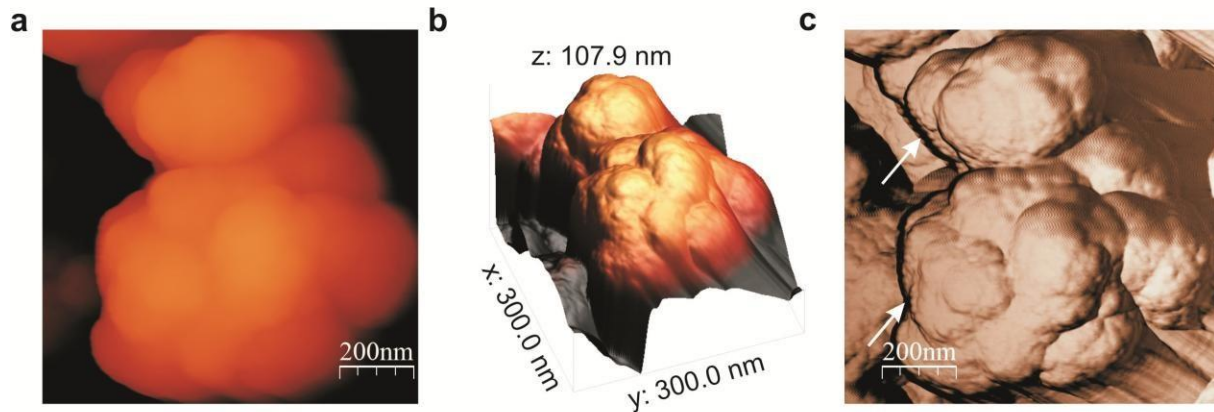


**Figure S4.** Nanoscale surface topography of a micrometer sized polymer globule on the MN-surface. **a**, AFM topography image, tapping mode, **b**, corresponding 3D representation, **c**, corresponding AFM phase image showing 20-30 nm features on the micrometer-sized polymer globules more clearly. Similar features are visible in SEM images.

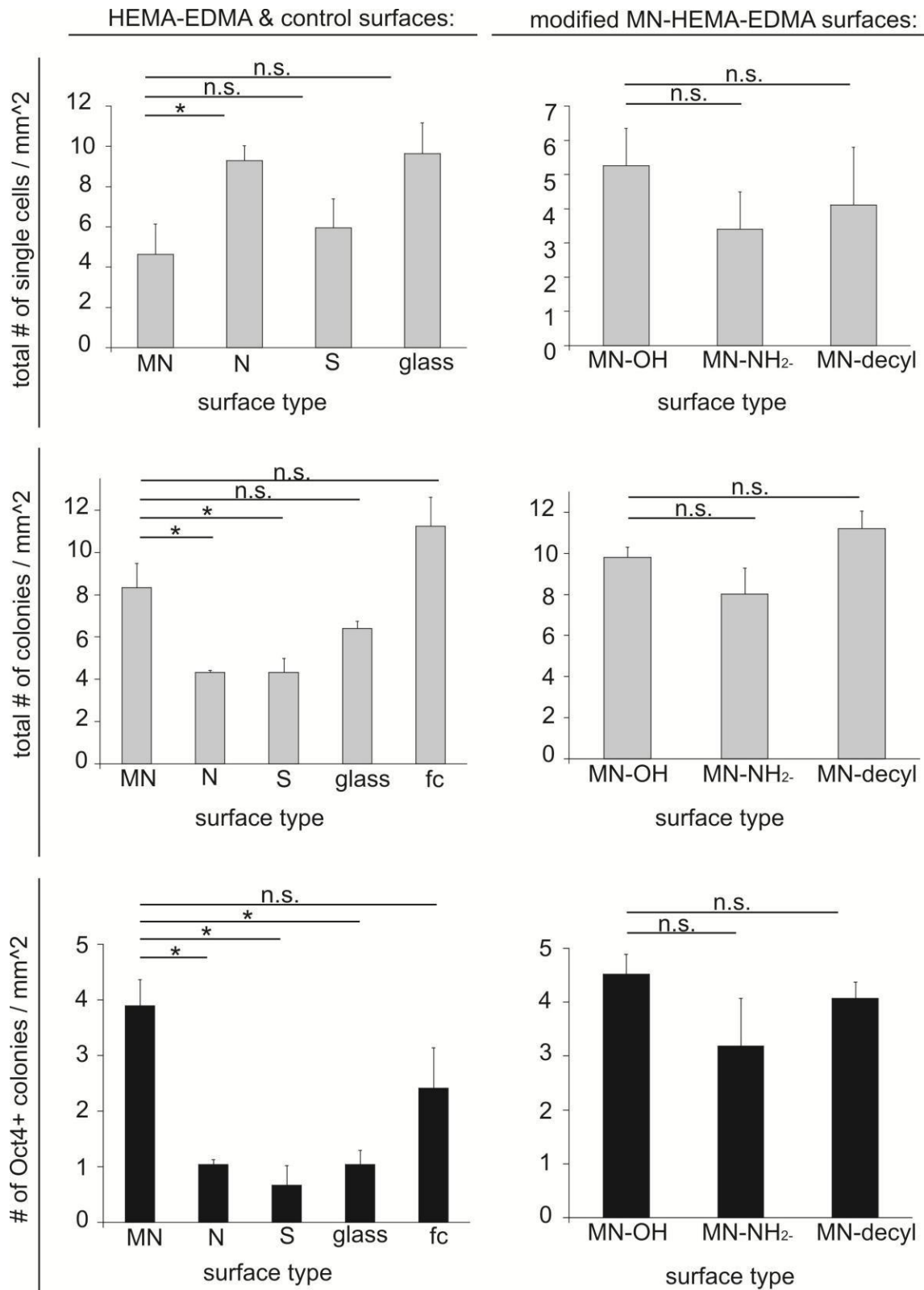


**Figure S5.** Count of single cells, total colony and Oct4+ colony number of Oct4-EGFP expressing mESCs on HEMA-EDMA-, modified HEMA-EDMA- and control surfaces. Evaluation was performed on fixed

and stained cells (DAPI, Phalloidin) after three days of culture. 15 images were evaluated per experiment and condition. Illumination times were equal per condition. A colony was defined by at least more than 10 connected cells. Error bars represent standard error of the mean.

Student's t-test (two-tailed); not significant (n.s.),  $p > 0.05$ ; \*,  $p \leq 0.05$ . N = 3, n > 100.

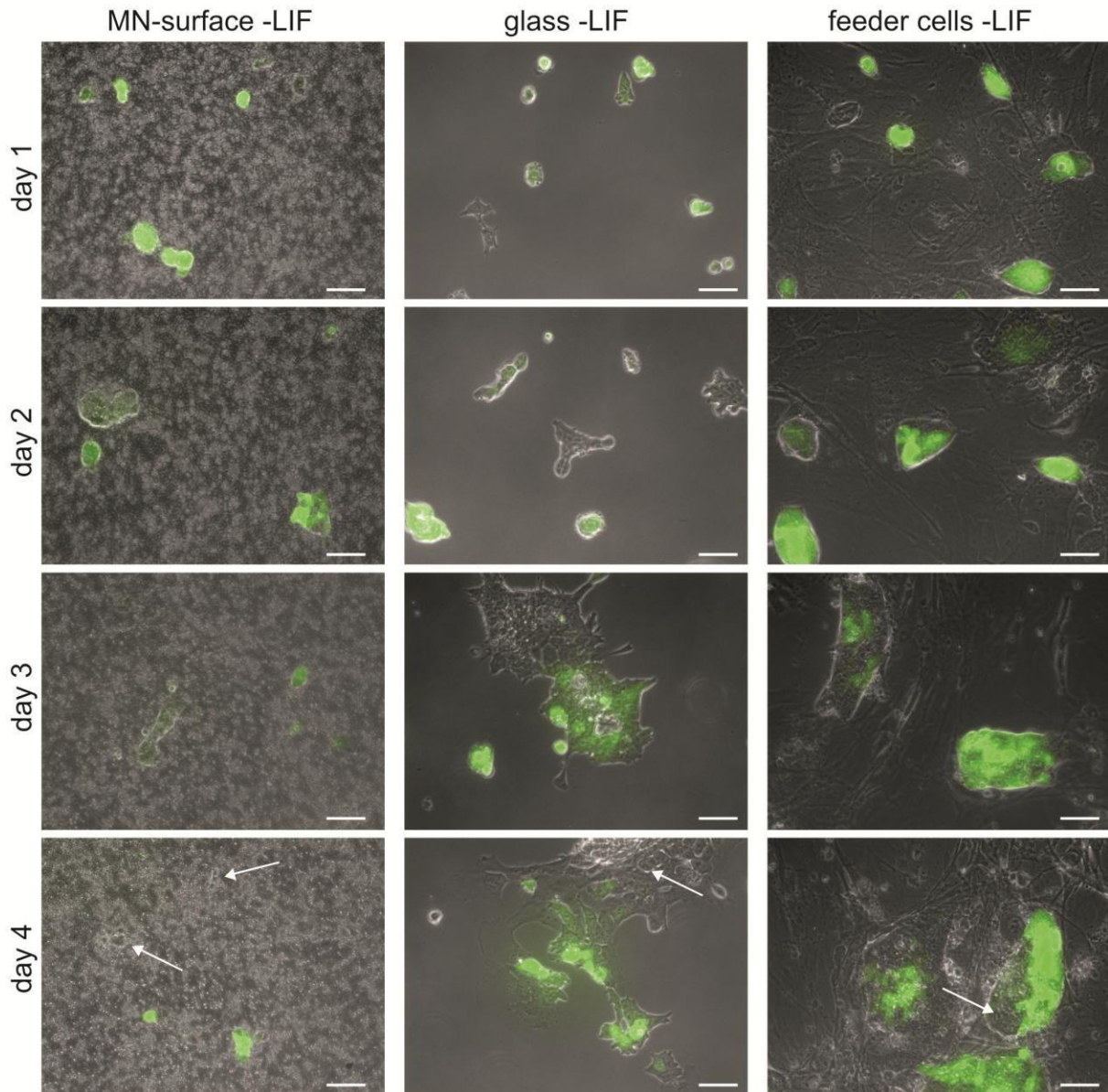


**Figure S6.** mESC growth and maintenance on MN- and control surfaces depends on LIF. Oct4-EGFP expressing mESCs were cultured in LIF-deprived medium for one, two, three and four days on a MNsurface, on glass or feeder cells. mESCs on glass and feeder cells lost their Oct4-level, cells on MNsurfaces failed to grow or to build large colonies and also lost Oct4-EGFP. Arrows: examples of Oct4negative cell clusters. Scale bar: 50  $\mu$ m.

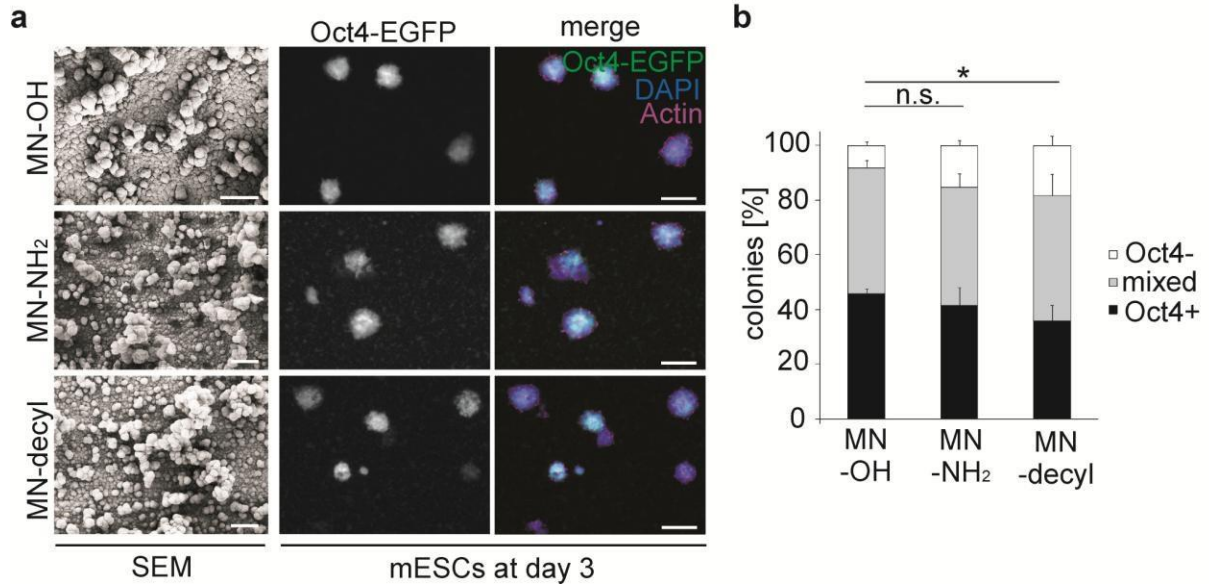


**Figure S7.** Oct4-EGFP expressing mESCs on modified MN-surfaces. **a**, The pristine hydroxylfunctionalized (-OH) MN-surfaces were chemically modified with amine (-NH<sub>2</sub>) or decyl terminal groups. Scanning electron microscopy (SEM) images show that the same surface roughness was maintained for non-modified, and amine or decyl-modified MN-surfaces. Oct4-EGFP (white/green) expressing mESCs were cultured for three days on MN-, MN-NH<sub>2</sub>, and MN-decyl surfaces and stained for their nuclei (DAPI) and actin cytoskeleton (magenta). Scale bars in the SEM images: 2  $\mu$ m; scale bars in the cell images: 100  $\mu$ m. **b**, Percentage of Oct4+ (black), Oct4- (white), and mixed (grey) mESC populations on non-modified, NH<sub>2</sub>- or decyl-modified MN-surfaces after three days of culture. Chi<sup>2</sup> test; not significant (n.s.),  $p > 0.01$ ; \*,  $p < 0.01$ . N = 3, n > 200. Error bars represent standard error of the mean.

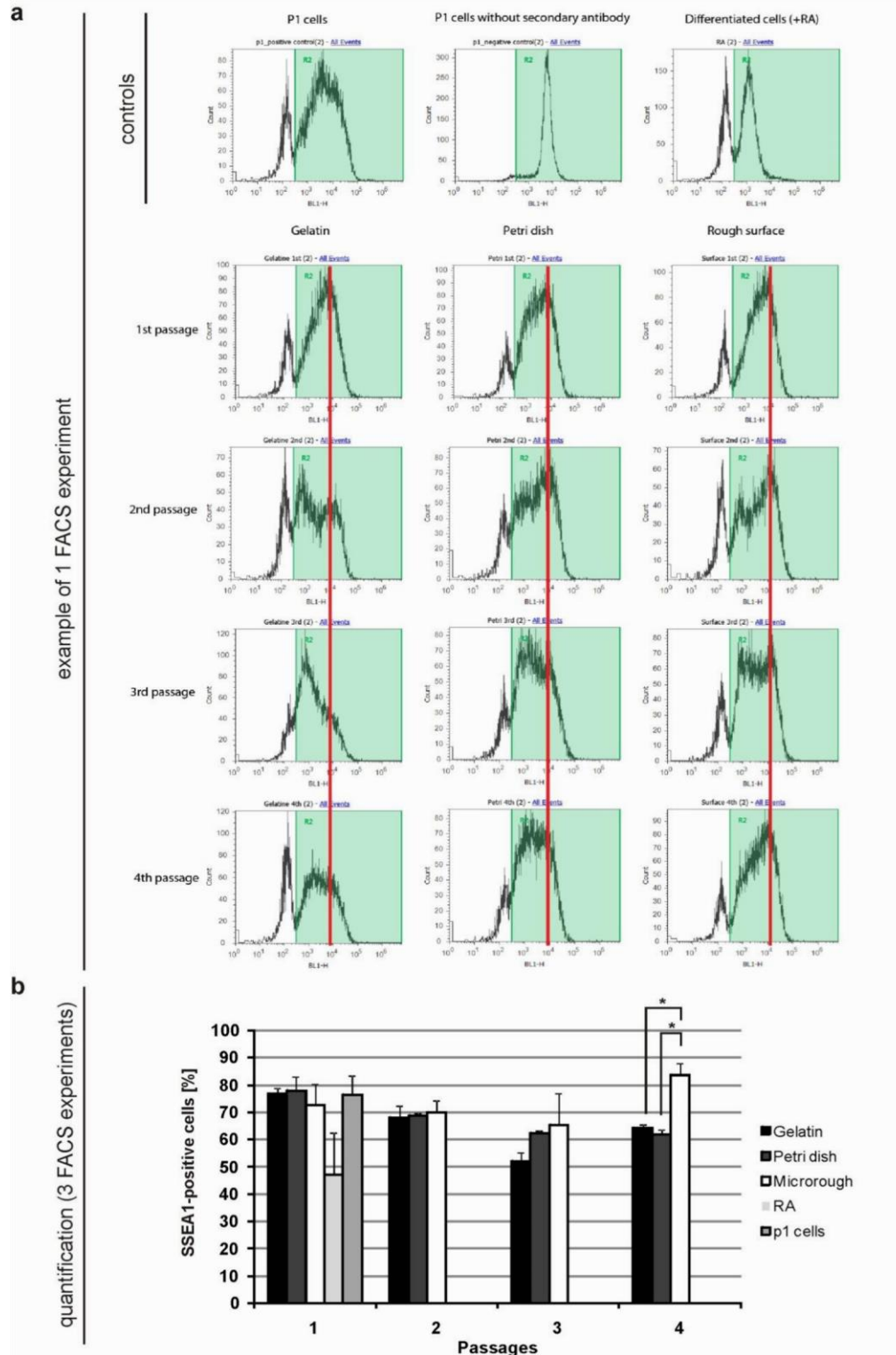


**Figure S8.** FACS analysis of D3 mESCs. **a**, D3 Cells (P1) were cultured for up to four passages (five days each) on micro-rough surfaces, Petri dishes or Petri dishes coated with gelatin. The cells were harvested, incubated with an antibody against SSEA1 and subsequently with an Alexa488-coupled secondary antibody. Cells were then analyzed by flow cytometry. D3 cells (P1) without addition of the secondary

antibody, or D3 cells differentiated by retinoic acid for five days (RA) served as negative control while D3 cells (P1) were used as positive control. **b**, The percentage of SSEA1-positive cells was quantified and plotted. Error bars represent standard error of the mean. Student's t-test (twotailed); \*,  $p \leq 0.05$ . N = 3.

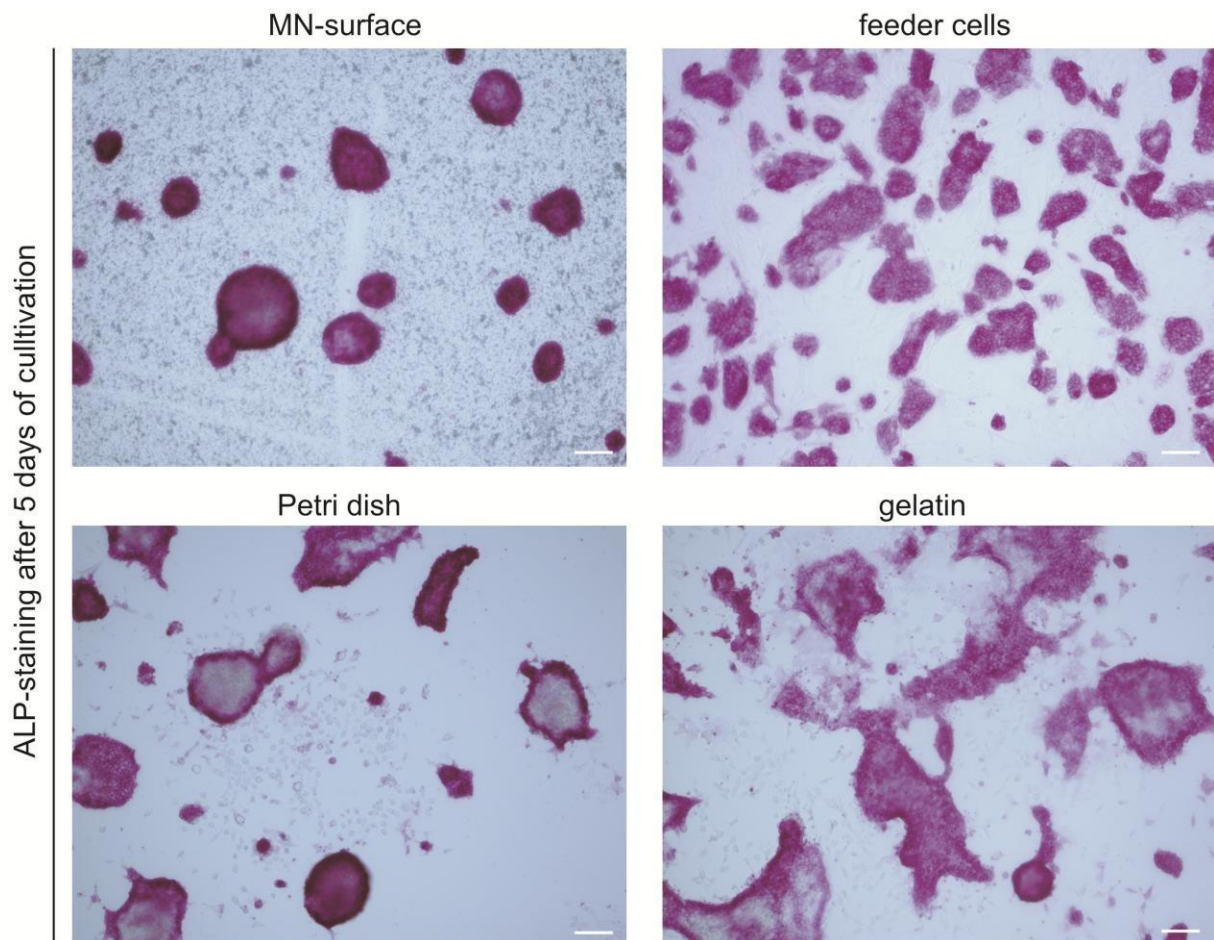


**Figure S9.** Alkaline phosphatase staining of D3 mESCs. The mESCs were cultivated for 5 days on a MN-surface, feeder cells and in a Petri dish with or without gelatin (two passages). They were fixed and stained for the pluripotency marker alkaline phosphatase (ALP). Colonies on the MN-surface exhibited round morphologies and were highly and regularly stained. On feeder cells, mESC colonies were less round, but showed a homogeneous ALP staining. In the non-coated Petri dish and on gelatin mESCs lost their ALP activity and migrated out of the colony formation; colonies also exhibited irregular and non-circular shapes. Furthermore, ALP staining was inhomogeneous with a strong staining at colony edges and a weak staining inside the colonies and in surrounding single cells. Scale bars: 50  $\mu$ m.

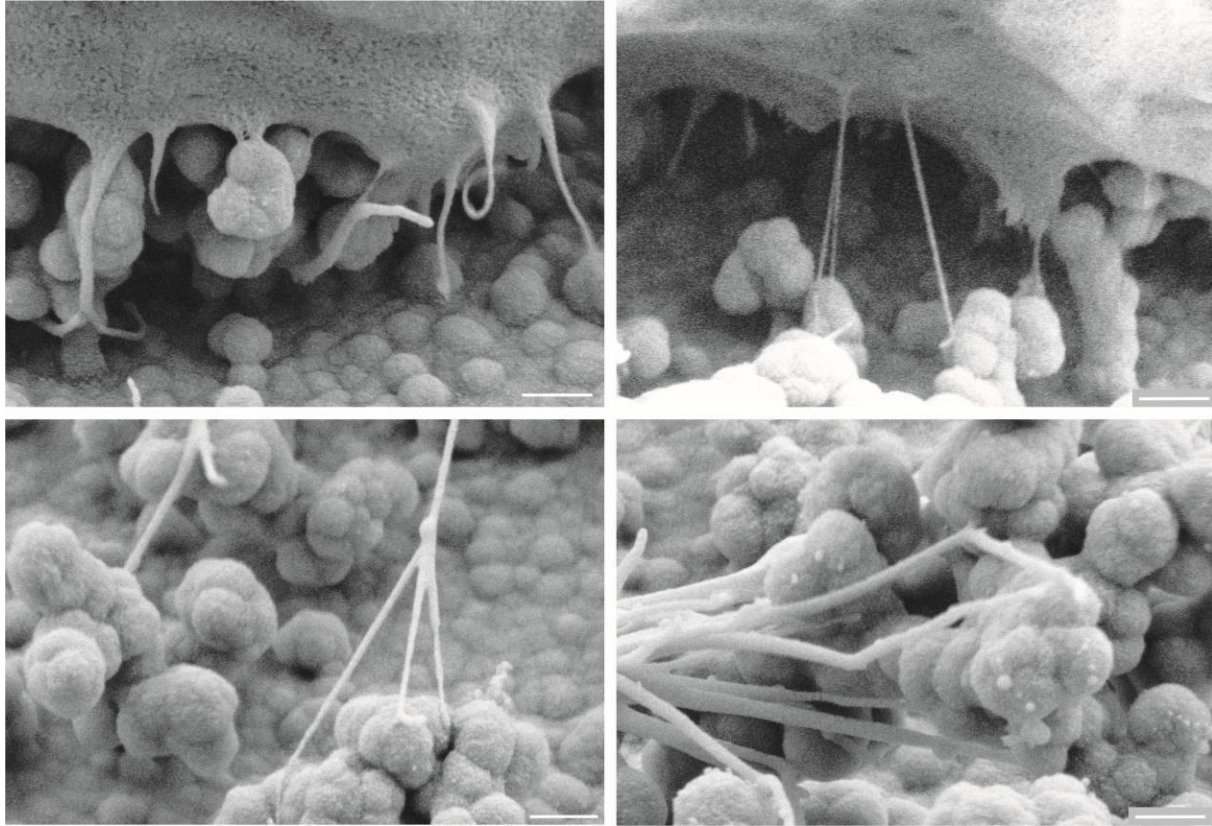


**Figure S10.** mESCs cultivated on MN-surfaces exhibit thin protrusions reaching into the MN-HEMAEDMA agglomerates. Scanning electron microscopic (SEM) images of the contact zone between Oct4-EGFP-expressing mESCs and MN-surfaces. Cells had been cultivated for 4 hours on the surfaces before fixation and imaging. Scale bars: 500 nm.

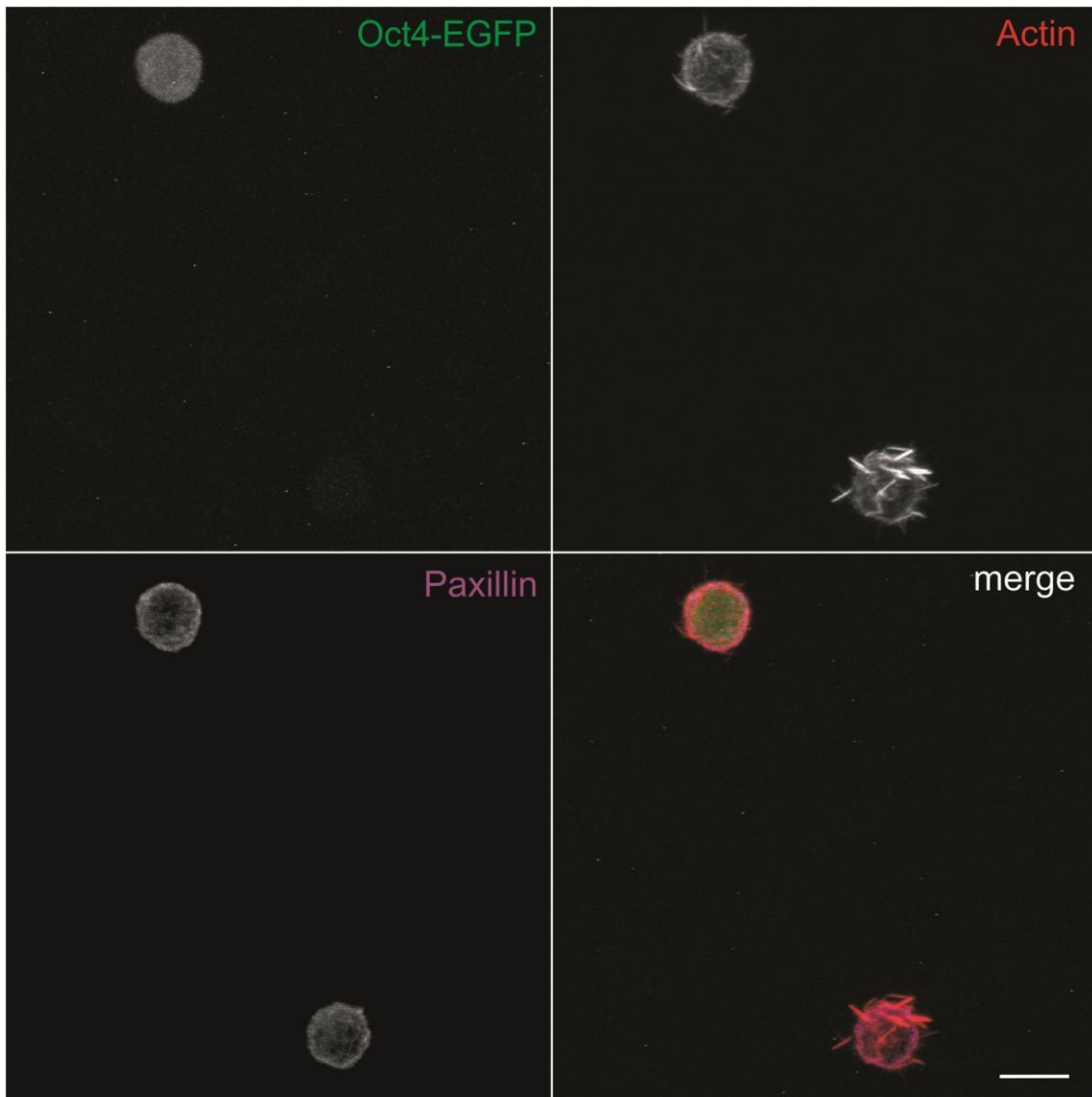


**Figure S11.** Example of an Oct4-positive (upper cell) and Oct4-negative (lower cell) cell of the Oct4EGFP mESC line, cultivated for 4 hours on a MN-surface. The cells were fixed and stained for actin (gray/red) and paxillin (gray/magenta). Actin protrusions and the absence of paxillin clusters occur in both cell types. Images show maximum intensity projections of LSM-scans. Scale bar: 10  $\mu$ m.

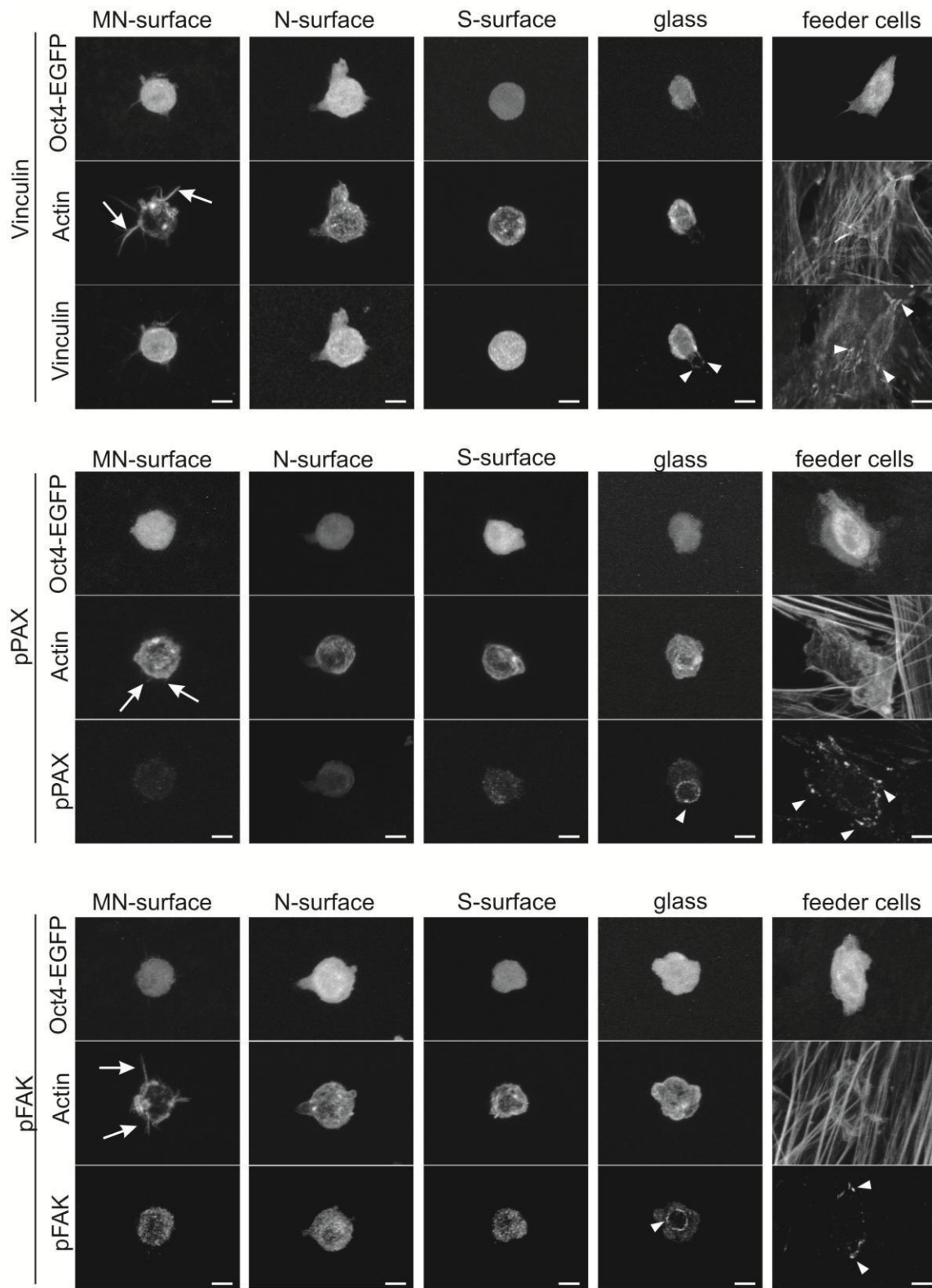


**Figure S12.** Analysis of single cell morphology and adhesion on HEMA-EDMA and control surfaces. Confocal images of single Oct4-EGFP expressing mESCs on different culture

substrates. The mESCs were stained for their actin cytoskeleton and vinculin (a marker for integrin-positive cell-matrix adhesion sites), phosphorylated paxillin (pPAX) or phosphorylated focal adhesion kinase (pFAK). pPAX and pFAK are markers for activated integrin signaling. Arrows indicate actin protrusions; arrowheads indicate vinculin-, pPAX- or pFAK-clusters, respectively. All images are maximum intensity projections. Scale bars: 5  $\mu$ m.

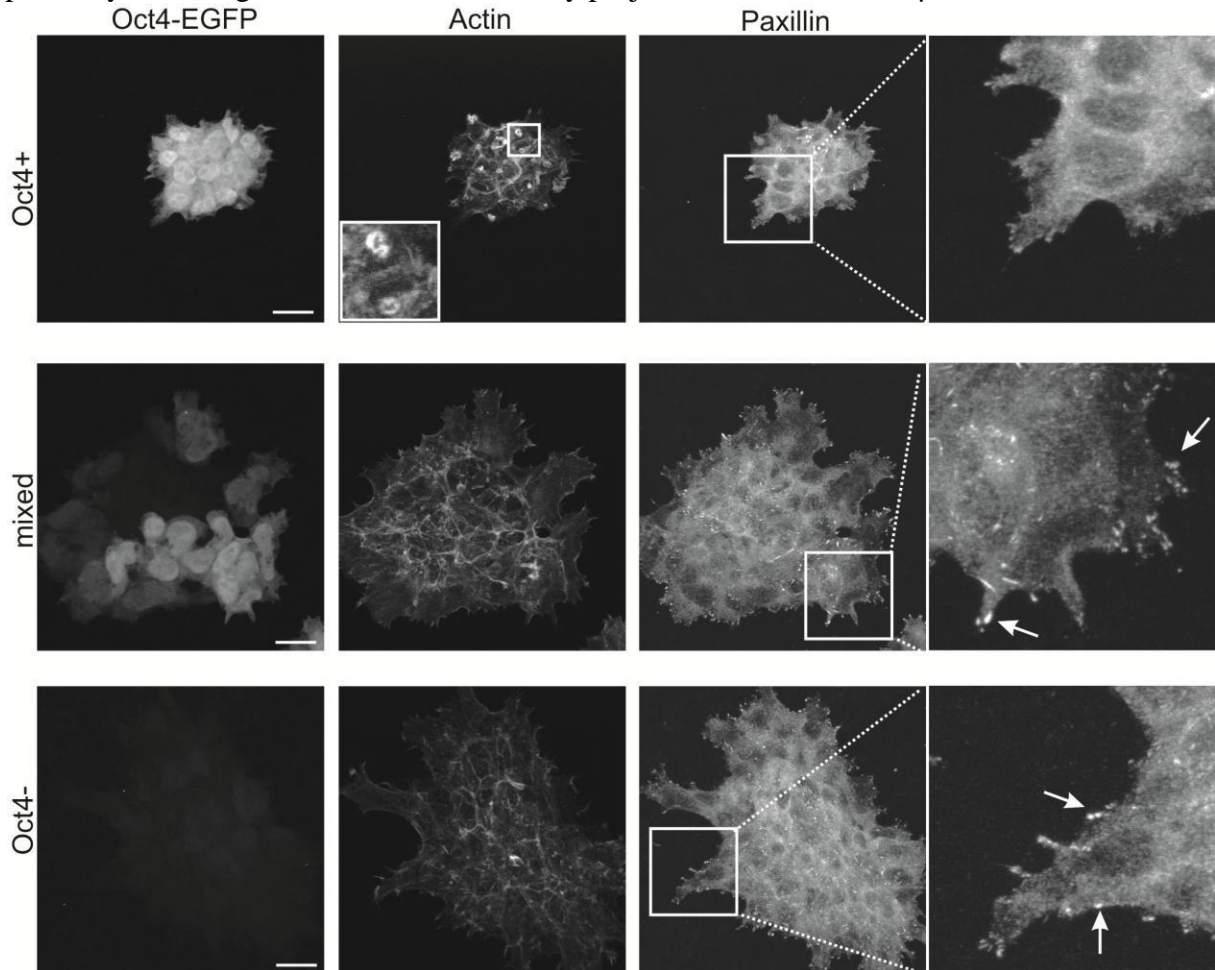


**Figure S13.** mESCs of the Oct4-EGFP line, cultivated for 3 days on a MN-surface. The cells were fixed and stained for their actin cytoskeleton and paxillin. Oct4+ colonies exhibit relatively large, ringshaped actin ruffles (inset) at the cell surface interface but rarely show paxillin clustering, whereas mixed and Oct4- colonies exhibit distinct paxillin clusters (arrows), especially on colony edges. Images show maximum intensity projections of LSM-scans. Scale bars: 20  $\mu$ m.

**Table S1.** Static and dynamic water contact angles (WCAs) of HEMA-EDMA surfaces. WCA values were obtained by a sessile drop measuring method. Dynamic WCA values were obtained by constantly pipetting and withdrawing milliQ on a polymer surface.  $\theta_{adv}$  = advancing WCA,  $\theta_{rec}$  = receding WCA,  $\theta_{static}$  = static WCA, CAH = contact angle hysteresis. Values represent mean  $\pm$  standard deviation.  $N \geq 3$ .

	MN-surface	N-surface	S-surface	MN-NH <sub>2</sub> surface	MN-decyl surface
$\theta_{adv}$	NA	27 $\pm$ 3°	60 $\pm$ 2°	27 $\pm$ 3°	164 $\pm$ 3°
$\theta_{static}$	<5°	15 $\pm$ 3°	57 $\pm$ 2°	20 $\pm$ 3°	160 $\pm$ 4°
$\theta_{rec}$	NA	13 $\pm$ 2°	39 $\pm$ 2°	17 $\pm$ 3°	148 $\pm$ 4°
CAH	NA	14°	21°	10°	16°

## Experimental procedures

### Fabrication of the MN-, N- and S- HEMA-EDMA surfaces

All chemicals and reagents for the production of HEMA-EDMA surfaces were purchased from Sigma-Aldrich at purity >97% if not designated differently in the text.

To create very thin micro-nano rough (MN-) surfaces a porous polymer was made by photopolymerization of a mixture containing 24wt% of the monomer 2-hydroxyethyl methacrylate (HEMA), 16wt% of the cross-linker ethylene dimethacrylate (EDMA), and 1wt% of the photoinitiator 2,2-dimethoxy-2-phenylacetophenon (DMPAP) in the presence of porogenic

solvents, 40wt% 1-decanol and 20wt% cyclohexanol. For covalent attachment of the polymer to the glass surface, the glass plates (Schott NexterionB) were modified with 3(trimethoxysilyl)propyl methacrylate (TMSPHA). The polymerization mixture was pipetted in a mold between two modified glass plates with 75  $\mu\text{m}$  thick Teflon spacers define polymer thickness. After 15 min UV-light irradiation (260 nm, 8mW/cm<sup>2</sup>) the two glass plates were separated by a scalpel. The hardened polymer broke into two polymer films attaching to both glass plates. The thin polymer layer attached to the bottom plate was washed with ethanol and acetone and dried with nitrogen. The samples were stored in methanol. For FNfunctionalization, MN-HEMA-EDMA surfaces were covered with 1 ml of a 10  $\mu\text{g}/\text{ml}$  fibronectin solution (diluted in 1xPBS pH 7.4) and incubated for 1 hour. Afterwards slides were rinsed with PBS.

Nano rough surfaces (N-surfaces) were prepared by photo-polymerization of a mixture containing 24wt% of the monomer HEMA, 16wt% of the cross-linker EDMA, 1 wt% of the photoinitiator DMPAP in the presence 12wt% 1-decanol and 48wt% cyclohexanol porogenic solvents. To ensure that the polymer attached only to the modified, glass slides were exposed to trichloro(1H, 1H, 2H, 2H-perfluorooctyl)silane in an evacuated desiccator overnight. The mixture was injected into a mold made of modified glass plate and a fluorinated glass plate, which were separated by two 12.5  $\mu\text{m}$  Teflon spacers. The mold was irradiated with UV-light (260 nm, 8 mW/cm<sup>2</sup>) for 15 min. Afterwards, the glass slides were opened with a scalpel and washed with methanol.

Smooth surfaces (S-surfaces) were prepared by photo-polymerization of a mixture containing 60wt% of the monomer HEMA, 40wt% of the cross-linker EDMA, and 1 wt%. of the photoinitiator DMPAP without any porogens and the substrates were processed like the N-surfaces.

### **Modification of MN-surfaces**

Alkyne-modified polymer layers were prepared by coating two glass plates with MN-HEMAEDMA surfaces. They were then immersed into 50 ml dichloromethane solution containing 1.14 mM 4-pentynoic acid and 0.46 mM 4-(dimethylamino)pyridine (DMAP)). 1.14 mM N,N'-diisopropylcarbodiimide (DIC) were added and the solution was cooled to 0°C. Then the solution was stirred at room temperature (RT) for 4 hours. The plates were washed extensively with acetone and were dipped into ethanol for several min. with subsequent air drying.

For amine (NH<sub>2</sub>)-modified MN-surfaces, an alkyne polymer layer was wetted with a Cysteamine hydrochloride (15 wt% in ethanol) solution covered with a fluorinated quartz slide (25×75×1 mm<sup>3</sup>, width×length×thickness), and irradiated with UV-light for 15s (12 mW/cm<sup>2</sup>, 260 nm). The samples were washed extensively with acetone and dried with nitrogen.

For the decyl-modified MN-surfaces the alkyne polymer layer was wetted with a 1decanethiol (5 vol% in acetone) solution covered with a fluorinated quartz slide (25×75×1 mm, width×length×thickness, developed with Autodesk Inventor 2011 software and manufactured by Rose Fotomasken), and irradiated with UV-light for 15s (12.0 mW/cm<sup>2</sup>, 260 nm) under ambient laboratory conditions. The samples were washed extensively with acetone and dried with nitrogen.

## **Characterization of the HEMA-EDMA surfaces**

Scanning electron microscopy (SEM): The surface morphologies of HEMA-EDMA polymer films and its derivatives were analyzed using the ZEISS Leo 1530 (Carl Zeiss NTS GmbH, Germany; (INT, KIT)) scanning electron microscope after gold sputtering (15 nm) using the Balzers Union MED 10 (INT, KIT).

Surface roughness measurements: Surface area profile was measured using Sensofar S neox (IAI, KIT). As the light source blue light was used (460 nm) and samples were analyzed using a 50x objective (NA 0.8, optical resolution 0.17  $\mu\text{m}$ , vertical resolution 3 nm).

Water contact angle measurements: Water contact angles (WCA) were evaluated with a UK1117 camera (EHD imaging GmbH, Germany), 5  $\mu\text{l}$  syringe (Hamilton, Switzerland) by a sessile drop measuring method. The advancing and receding WCAs were determined by consecutive addition and subtraction of MilliQ water to the droplet. The measurements of WCAs were repeated at least three times. The calculation of WCA was performed using ImageJ Drop Analyzer plug-in (<http://imagej.nih.gov/ij/>).

Atomic Force Microscopy (AFM): All AFM measurements were performed using a Dimension Icon (Bruker, Karlsruhe, Germany) with HQ:NSC15/AL BS tips ( $\mu\text{Masch}$ ) in tapping mode.

## **Oct4-EGFP expressing mESCs**

Oct4-EGFP expressing mouse embryonic stem cells were kindly provided by Prof. Rolf Kemler (MPI, Freiburg). Briefly, homozygous mice of the Oct4-EGFP mouse strain<sup>1</sup> were crossbred with female C57BL/6 mice. Animal housing conditions fulfilled the animal welfare guidelines. Morulae were isolated at day 2.5 post-fertilization and cultivated in KSOM mouse embryo medium under standard cell culture conditions. Morulae were enzymatically dissociated and resulting cells and cell clusters were initially cultivated on mitotically inactivated feeder cells in the presence of a MEK5 inhibitor to prevent differentiation. Experiments were performed according to European (Council Directive 86/609/EEC) and German (Tierschutzgesetz) guidelines for the welfare of experimental animals.

## **Routine culture of mESCs**

Oct4-EGFP expressing mESCs were cultured in high glucose DMEM supplemented with 15% PANsera ES (PAN Biotech), 1 mM sodiumpyruvate, 2 mM L-glutamine, 1x NEAA, 0.1 mM  $\beta$ -mercaptoethanol, LIF (80  $\mu\text{l}$  cell culture supernatant of HEK293 cells stably transfected with a LIF expression plasmid per 5 ml of mESC culture media) and 1-3% penicillin/streptomycin on a confluent layer of primary mouse embryonic fibroblasts (obtained from Doris Wedlich, KIT) that had been mitotically inactivated with 10  $\mu\text{g/ml}$  Mitomycin C for 2 to 3 hours and seeded in culture flasks coated with 0.1% porcine gelatin in PBS. Cells were cultivated at 37°C, 7% CO<sub>2</sub> and 95%

humidity and passaged every second day. For experiments, cells with passage numbers below 20 were used.

The mouse embryonic stem cell line D3 (derived from a 129S2/SvPas mouse from ATCC) was cultured in GlutaMAX™-1 medium (Invitrogen) supplemented with 15% ES FBS (PAA), 0.1mM β-mercaptoethanol, 1% penicillin/streptomycin and 1000 units/ml LIF at 37°C/5% CO<sub>2</sub>/95% humidity. Mouse embryonic fibroblasts (MEFs) that had been irradiated with 6.3 Gray served as feeder cells. Medium was changed every day and cells were split at least every second day.

### **Pre-plating of Oct4-EGFP expressing mESCs**

In order to separate mESCs from MEF-feeder cells prior to experiments the mixture of cells was transferred into non-coated cell culture flasks with 5 ml of stem cell medium supplemented with LIF. The flasks were incubated in 37°C to let feeder cells adhere to the surface. The mESCs which adhere much slower to non-coated cell culture flasks, were collected after 30 to 60 min and transferred to a new culture flask coated with 0.1% gelatin and incubated for a maximum of two days before usage in experiments.

### **Cultivation of mESCs on HEMA-EDMA surfaces**

For cultivation of mESCs on MN-, N- and S-HEMA-EDMA surfaces, the surfaces were sterilized by rinsing with 70% ethanol and dried in a clean bench. The polymer-coated glass plates and control surfaces (glass coverslips, with and without mitotically inactivated feeder cells) were transferred into a six-well plate with 2 ml of medium per well supplemented with LIF.  $5 \times 10^4$  -  $8 \times 10^4$  of the pre-plated and singularized stem cells were transferred to the substrates and incubated between 4 hours (for single cell analysis) and 5 days (for time series) with a medium change every second or third day. For long term cultivation, mESCs on MNsurfaces were passaged every third or fourth day by trypsinizing them with Trypsin/EDTA, diluted 1:1 in Hank's Buffered Salt Solution (HBSS) for five minutes with subsequent shaking to get the strongly adhering cells off the surface. They were then cultivated on new sterilized substrates. In case of mESCs adhering to feeder cells, a 1:4 dilution of Trypsin/EDTA in HBSS applied for 3 minutes was sufficient to passage the cells.

### **Image acquisition of living mESCs**

Stem cell colonies (of the Oct4-EGFP line) on different surfaces were imaged regularly at an Axio Imager.Z1 equipped with an Achromplan 20x/0.50W Ph2 dip-in objective (Carl Zeiss) and an AxioCamMRm (Carl Zeiss). The medium was changed after each imaging session in order to avoid contamination.

For long term cultivation images were taken immediately before passaging.

### **Alkaline phosphatase staining of mESC line D3**

Cells of the mESC line D3 were washed twice with PBS and fixed by 2 ml of 4% paraformaldehyde in PBS for 20 min. Thereafter, cells were washed three times with 5 ml Tris-maleate buffer (1 M maleic acid, 0.02 M Tris, pH 9.0) for 5 min. The activity of alkaline phosphatase was developed by incubation with the reaction buffer (0.1% Fast Red TR Salt, 0.02% Naphtol AS-MX Phosphate, and 0.08% MgCl<sub>2</sub> in Tris-maleate buffer) for 10-20 min.

The positive clones (stained in red) were visualized by light microscopy.

### **Flow cytometry of mESC line D3**

4x10<sup>5</sup> cells of the mESC line D3 were harvested in a 1.5 ml Eppendorf tube and washed twice with 500 µl ice-cold FACS buffer (0.1% FCS in PBS). Cells were then suspended in 200 µl solution of primary antibody SSEA1 (monoclonal mouse anti-SSEA1 (Santa Cruz, 1:100 dilution in 5% BSA/PBST), and incubated overnight at 4°C. Cells were washed three times by centrifugation at 400 g for three min in ice cold FACS buffer. Afterwards, cells were resuspended in 200 µl solution of Alexa Fluor 488-labeled secondary antibody (Alexa Fluor 488 goat anti-mouse IgG (Invitrogen)) (1:100 dilution in 5% BSA/PBST), and incubated overnight at 4°C in the dark. Cells were fixed with 100 µl 3.7% paraformaldehyde for 10 min, and then filled up with 1.2 ml FACS buffer. Cell suspension was stored immediately at 4°C in the dark until they were measured by Attune Acoustic Focusing Cytometer (Life Technologies).

### **Western blotting of mESC line D3**

D3 mES cells were washed with PBS, and lysed in NP40 lysis buffer (50 mM Tris pH 8.0, 150 mM NaCl, 5 mM EDTA, 1% NP40, 1mM PMSF) for 10 min on ice. The protein extract was cleared by centrifugation at 13,000 g for 10 min at 4°C. Then, the protein concentration of the cell lysate was determined by the method of Bradford. For SDS-PAGE and Western blotting 30 µg of total protein in 1x sample buffer (2% sodiumdodecylsulfate (SDS), 80 mM Tris pH 6.8, 10% glycerol, 5% 2-mercaptoethanol, 0.001% bromophenol blue) were heated for 5 min at 95°C, loaded onto an SDS-10% polyacrylamide gel, separated by electrophoresis and transferred onto a polyvinylidenedifluoride membrane (Millipore) using the Trans-Blot Turbo semi-dry transfer system (Bio-Rad). The membrane was blocked for 60 min in 5% BSA in PBST (0.2% Tween-20 in PBS) and incubated overnight at 4°C with the primary antibodies (polyclonal rabbit anti-Nanog (Serotec); monoclonal mouse anti-Oct3/4 (H-300) (Santa Cruz), and mouse monoclonal anti-β-Actin (Abcam)). After washing 3 times for 5 min in PBST, the secondary antibodies conjugated with horseradish peroxidase (HRP) (goat antimouse IgG/HRP and Goat anti-rabbit IgG/HRP (both from Dako)) were added and incubated for 1 hour. After extensive washing, the blots were developed by adding ECL (Pierce ECL Western Blotting substrate) and exposing the membranes against an X-ray film.

## **Scanning electron microscopy of Oct4-EGFP-expressing mESCs cultivated on different surfaces**

Cells on different surfaces were fixed after 4 hours of cultivation in 2% PFA and 2% glutaraldehyde (Sigma Aldrich) in PBS for at least 1 hour at RT. The samples were dehydrated by incubating them successively for 10 min in 10, 30, 50, 70, 90 and finally 3 times in 100% of acetone respectively. They were stored in 100% acetone before critical point drying. Critical point drying was performed with an EM CPD030 (Leica) with acetone as substitution liquid. The samples were flushed with liquid CO<sub>2</sub> for 6-8 times and dried at 40°C and 75 bar. The dried samples were glued onto a sample holder and coated with a thin layer (3-5 nm) of gold. SEM imaging was performed by using a LEO 1530 Field Emission Scanning Electron Microscope.

**Immunofluorescence staining of Oct4-EGFP-expressing mESCs and confocal imaging** The cells were fixed with 4% paraformaldehyde (PFA, Sigma Aldrich) in PBS for 10 min. After permeabilization with PBS containing 0.1% Triton, cells were incubated with the primary antibody (mAb IgG mouse anti-Paxillin, 1:500, BD Transduction Laboratories; mAb IgG mouse anti-Vinculin, 1:100, Abcam; pAb IgG rabbit anti-Phospho-Paxillin pTyr31, 1:500, Life Technologies; pAb IgG rabbit anti-Phospho-FAK pTyr397, 1:300, Life Technologies) for 1 hour at RT. Samples were washed 3 x 5 min with PBS and subsequently incubated with the secondary antibody (goat anti-mouse IgG AlexaFluor 647, 1:200, Dianova; goat anti-rabbit IgG Cy3, 1:200, Dianova) in 1% BSA in PBS at RT for 1 hour together with phalloidin-AlexaFluor568 (1:200, Molecular Probes) or phalloidin-AlexaFluor647 (1:200, Molecular Probes) and DAPI (1:1000, Roth). Samples were washed 3 x 5 min with PBS and embedded in 1% n-propylgallate (Sigma Aldrich) in Mowiol (Hoechst).

Confocal imaging was performed with a LSM 510 Meta microscope (Carl Zeiss) equipped with a LCI Plan-Neofluar 63x/1.3 DIC IM Korr objective (Carl Zeiss).

## **Analysis**

For the estimation of single cell number, colony pluripotency and colony numbers, cells were seeded, cultivated for 3 days and stained as described above. 15 images per condition were taken randomly at an Axio Imager.Z1 equipped with an EC Plan NEOFLUAR 10x/0.3 Ph1 Objective and an AxioCamMRm (all from Carl Zeiss). Exposure times were identical for each channel in all conditions. Single cells and colonies (defined as more than ten connected cells) were counted with the help of the nuclear and actin-staining in all 15 images. For colonies, the pluripotency state was determined with the intrinsic Oct4-EGFP signal. Colonies were classified into Oct4-EGFP-positive (all cells fluorescent at the given illumination time), Oct4EGFP-negative (no fluorescent cells present) and mixed (fluorescent and non-fluorescent cells present in one colony).

To assess mESC colony circularity, Oct4-EGFP images of the long term cultivation experiment were evaluated by the analyze particles tool from ImageJ

(<http://imagej.nih.gov/ij/>) for 15-20 colonies per time point and condition.

For the quantification of the Western Blot, signals for Oct4, Nanog and  $\beta$ -Actin were quantified densitometrically via ImageJ and the relative amounts of Oct4 and Nanog were assessed by correlating it with the  $\beta$ -Actin signal. Relative abundance of Oct4 and Nanog proteins at the 1<sup>st</sup> passage was set to 1.

### **Statistics**

For each experimental set (except of the circularity data) at least three independent experiments have been performed. The circularity data and Western Blot quantification were obtained from one experiment. All data were expressed as means  $\pm$  standard error of the mean (s.e.m.) if not designated differently. Excel 2007 (Microsoft Corporation, Redmont, USA) was used for statistical analysis (two-tailed Student's t-test or a Chi<sup>2</sup> test, respectively). Differences were considered as statistically significant when the calculated p value was less than 0.05 (\*) and a p value above 0.05 was considered non-significant (n.s.) for Student's ttest. For the Chi<sup>2</sup> test, the critical significance value was set to  $p < 0.01$ .

### **References**

- 1) Kirchhof, N.; Carnwath, J. W.; Lemme, E.; Anastassiadis, K.; Schöler, H.; Niemann, H.; *Biol. Reprod.* **2000**, *63*, 1698-1705.